Research Articles

Atmospheric Constraints on the Surface UV Environment of Mars at 3.9 Ga Relevant to Prebiotic Chemistry

Sukrit Ranjan,[1] Robin Wordsworth,[2,3] and Dimitar D. Sasselov[1]

Abstract

Recent findings suggest that Mars may have been a clement environment for the emergence of life and may even have compared favorably to Earth in this regard. These findings have revived interest in the hypothesis that prebiotically important molecules or even nascent life may have formed on Mars and been transferred to Earth. UV light plays a key role in prebiotic chemistry. Characterizing the early martian surface UV environment is key to understanding how Mars compares to Earth as a venue for prebiotic chemistry.

Here, we present two-stream, multilayer calculations of the UV surface radiance on Mars at 3.9 Ga to constrain the surface UV environment as a function of atmospheric state. We explore a wide range of atmospheric pressures, temperatures, and compositions that correspond to the diversity of martian atmospheric states consistent with available constraints. We include the effects of clouds and dust. We calculate dose rates to quantify the effect of different atmospheric states on UV-sensitive prebiotic chemistry.

We find that, for normative clear-sky CO_2-H_2O atmospheres, the UV environment on young Mars is comparable to young Earth. This similarity is robust to moderate cloud cover; thick clouds ($\tau_{cloud} \geq 100$) are required to significantly affect the martian UV environment, because cloud absorption is degenerate with atmospheric CO_2. On the other hand, absorption from SO_2, H_2S, and dust is nondegenerate with CO_2, meaning that, if these constituents build up to significant levels, surface UV fluence can be suppressed. These absorbers have spectrally variable absorption, meaning that their presence affects prebiotic pathways in different ways. In particular, high SO_2 environments may admit UV fluence that favors pathways conducive to abiogenesis over pathways unfavorable to it. However, better measurements of the spectral quantum yields of these pathways are required to evaluate this hypothesis definitively. Key Words: Radiative transfer—Origin of life—Mars—UV radiation—Prebiotic chemistry. Astrobiology 17, 687–708.

1. Introduction

RECENT FINDINGS suggest that young Mars may have been a clement environment for the emergence of life. Analysis of Curiosity imaging of sedimentary rock strata deposited 3.2–3.6 Ga (Grotzinger *et al.,* 2015) suggests individual lakes were stable on ancient Mars for 100 to 10,000 years, with fluvial features laid down over 10,000 to 10 million years assuming formation rates that correspond to modern Earth. Similarly, Curiosity measurements of olivine and magnetite at Yellowknife Crater are consistent with aqueous conditions at near-neutral pH for thousands to hundreds of thousands of years in the Noachian, with an oxidant supply that could be an energy source (Bristow *et al.,* 2015). In general, the geological evidence is compelling that liquid

water, a requirement for life as we know it, was present on Mars at least transiently in the Noachian (Wordsworth, 2016).

Young Mars may also have been a favorable environment for prebiotic chemistry (chemistry relevant to the origin of life). Meteorite analysis has detected boron in martian clays, which is important for abiogenesis since borate minerals can stabilize ribose and catalyze other prebiotic chemistry reactions (see Stephenson *et al.,* 2013, and sources therein). Mars may also have had a greater availability of prebiotically important phosphate than was the case for Earth (Adcock *et al.,* 2013). Climate models suggest that liquid water was transient on Mars (Wordsworth *et al.,* 2013), which suggests the existence of wet/dry cycles. Such cycles are useful for prebiotic chemistry; aqueous eras are

---

[1]Harvard-Smithsonian Center for Astrophysics, Cambridge, Massachusetts.
[2]Harvard Paulson School of Engineering and Applied Sciences, Harvard University, Cambridge, Massachusetts.
[3]Department of Earth and Planetary Sciences, Harvard University, Cambridge, Massachusetts.

beneficial for the formation of biotic monomers, while dry eras tend to concentrate feedstock molecules and aid monomer polymerization (Benner and Kim, 2015), all of which is relevant to the formation of nucleotides and amino acids (Patel *et al.,* 2015). Finally, the putative dryness of Mars and the potential acidity of its early aqueous environment owing to dissolved carbonic acid from a CO_2-dominated atmosphere suggest that molybdate, which is suggested to catalyze formation of prebiotically important sugars such as ribose, may have been stable on Mars (Benner *et al.,* 2010; Benner and Kim, 2015). Hence, there is growing interest in the possibility that prebiotically important molecules may have been produced on Mars (Benner, 2013), and in the hypothesis that life may have originated on Mars and been seeded to Earth (Kirschvink and Weiss, 2002; Gollihar *et al.,* 2014; Benner and Kim, 2015).

Ultraviolet light plays a key role in prebiotic chemistry. UV photons can dissociate molecular bonds, produce ionic species, and excite molecules. These properties mean that UV light can stress prebiotic molecules (Sagan, 1973) but can also power synthetic prebiotic photochemistry. UV light has been invoked in prebiotic chemistry as diverse as the origin of chirality (Rosenberg *et al.,* 2008), the synthesis of amino acid precursors (Sarker *et al.,* 2013), and the polymerization of RNA (Mulkidjanian *et al.,* 2003).

The last decade has seen breakthroughs in long-standing problems in prebiotic chemistry such as the discovery of plausible mechanisms for the abiotic formation of activated pyrimidine ribonucleotides (Powner *et al.,* 2009), the synthesis of short (2- and 3-carbon) sugars (Ritson and Sutherland, 2012), and a reaction network generating precursors for a range of prebiotically important molecules including lipids, amino acids, and ribonucleotides (Patel *et al.,* 2015). These pathways all require UV light to function. In experiments, line sources such as low-pressure mercury lamps with monochromatic 254 nm emission are often used to simulate the incident UV radiation. However, prebiotic UV radiance in CO_2-dominated terrestrial-type atmospheres should instead be characterized by access to broadband fluence (Ranjan and Sasselov, 2017). The difference can have a significant impact on prebiotic chemistry (Ranjan and Sasselov, 2016), and there is a growing awareness in the prebiotic community of the importance of characterizing the wavelength dependence of proposed prebiotic pathways and/or using broadband sources in simulations (Rapf and Vaida, 2016). Consequently, it is important to constrain the UV environment on the surface of Mars at epochs relevant to potential prebiotic chemistry on a spectral (wavelength-dependent) basis.

In this work, we used a two-stream multilayer radiative transfer model to constrain the surface UV environment on young Mars (3.9 Ga). We calculated the surface radiance as a function of solar zenith angle (SZA), surface albedo (A), and atmospheric composition. Our model can calculate absorption and scattering due to eight gaseous species (CO_2, H_2O, CH_4, SO_2, H_2S, O_2, and O_3) and three particulate species (H_2O ice, CO_2 ice, and martian dust). Earlier analyses have focused on clear-sky "case studies" for the atmospheric composition; we instead explore the full range of martian atmospheric states consistent with available geological data and climate/photochemical modeling for the

martian atmosphere. We convolve the calculated surface radiance spectra against action spectra that correspond to two different simple photochemical reactions (one useful to prebiotic chemistry and one detrimental) that may have been important during the era of abiogenesis, and integrate the result to compute the biologically effective dose rate and estimate the impact of these parameters on prebiotic chemistry.

In Section 2, we discuss previous work on this topic. In Section 3, we describe our radiative transfer model and its inputs and assumptions. Section 4 presents the surface radiances calculated from our model as a function of martian atmospheric state, and in Section 5 we discusses the implications for prebiotic chemistry. Section 6 summarizes our findings.

2. Background

Recognizing the importance of UV light to life (though mostly in the context of a stressor), previous workers have placed constraints on the primitive martian surface UV environment. In this section, we present a review of previous work on this topic and discuss how our work differs from theirs.

Cockell (2000) calculated the martian surface flux at 3.5 Ga assuming solar input of 0.75× modern and an atmosphere composed of 1 bar CO_2 and 0.1 bar N_2. He computed his radiative transfer in a cloud-free atmosphere using a monolayer two-stream approximation with Delta-Eddington closure. He ignored water absorption, but a dust optical depth of 0.1 was assumed, as is a Lambertian surface with surface albedo $A = 0.1$. Cockell (2000) reported the total irradiance as a function of solar time (equator at equinox) as well as the biologically weighted[1] irradiance for DNA inactivation and photosystem damage, but not the spectral irradiance (for the early Mars case). He found the DNA inactivation-weighted irradiance to be comparable for his models of Early Mars and Early Earth, leading him to suggest that, from a UV perspective, the two worlds were comparably habitable.

Rontó *et al.* (2003) calculated the martian surface flux at 3.5 Ga from 200 to 400 nm. They assumed a 1 bar CO_2 atmosphere overlying volatilizable surface H_2O and ran it through the PHOEBE photochemical model to generate atmospheric profiles for the other molecules that would be generated. They found that a significant population of spectrally absorbing O_2, O_3, and NO_2 would be generated, including an ozone shield comparable to that of modern Earth. They evaluated radiative transfer for both a pure CO_2 atmosphere and an atmosphere with the trace species calculated in their photochemical model. Their UV radiative transfer models assume pure absorption and ignore scattering. In this formulation, Rontó *et al.* (2003) calculated Rayleigh scattering cross sections but treated them as absorption cross sections. This approach strongly overestimates attenuation at scattering wavelengths. It is consequently unsurprising that Rontó *et al.* (2003) reported strong attenuation of surface UV fluence for both model atmosphere cases. In the full photochemical model case,

---

[1]A measure of reaction rate; see Section 3.4.

fluence shortward of 290 nm is completely removed, due to the buildup of an ozone layer from CO_2 photolysis. However, Segura *et al.* (2007) noted that this photochemical model neglects a supply of reducing gases to the atmosphere due to volcanism and sinks of oxic gases related to processes that involve rainout; including either of these effects prevents the formation of an ozone layer. Geological evidence (*e.g.,* the Tharsis plateau) indicates that young Mars had significant volcanism, which would have prevented the formation of an ozone layer of the type calculated by Rontó *et al.* (2003).

Cnossen *et al.* (2007) calculated the martian surface flux from ~3.5 to 4 Ga assuming a 5 bar CO_2, 0.8 bar N_2 clear-sky atmosphere. They used shortwave observations of the solar analog κ^1 ceti combined with a scaled solar spectrum at longer wavelengths as their top-of-atmosphere (TOA) solar input. To calculate radiative transfer, they partitioned the atmosphere into 40 layers. They computed absorption using the Beer-Lambert law. To account for scattering, they computed the flux scattered in each layer, assumed half of it proceeds downward and half of it proceeds upward, and iterated this process to the surface. This approach implicitly neglects multiple scattering and assumes a surface albedo of 0 and, hence, tends to overestimate atmospheric attenuation of incoming radiation. Hence, Cnossen *et al.* (2007) reported broadband suppression of the TOA flux by multiple orders of magnitude.

Our work builds on these previous efforts. Like Cockell (2000), Rontó *et al.* (2003), and Cnossen *et al.* (2007), we consider the effects of a denser CO_2 atmosphere; however, we consider a broader range of surface atmospheric pressures permitted by available constraints, ranging from 2×10^{-5} to 2 bar. We build on the Cockell (2000) monolayer two-stream approach to radiative transfer by using a multiple-layer two-stream model, which consequently accounts for the effects of multiple scattering. Such a treatment is essential because of the unique radiative transfer regime unveiled in thick anoxic atmospheres (*e.g.,* multibar CO_2 atmospheres) at UV wavelengths, characterized by the atmosphere being simultaneously optically thick and scattering-dominated. In this regime, multiple-scattering dominates, and it is critical to account for its effects in order to compute surface radiation environments. As a corollary, the radiative transfer treatments of Rontó *et al.* (2003) and Cnossen *et al.* (2007) are not valid in this regime[2].

In addition to varying levels of CO_2, our work also explores the impact of other potential atmospheric constituents on the surface UV environment. In particular, we focus on the effect of enhanced concentrations of volcanogenic gases (*e.g.,* SO_2, H_2S), which may have been present at elevated levels on early Mars (Halevy *et al.,* 2007; Halevy and Head, 2014) and, if present, could have had a dramatic effect on the surface fluence (Ranjan and Sasselov, 2017). We also explore the radiative impact of varying levels of dust and CO_2 and H_2O clouds in the martian atmosphere, which may have been abundant (Wordsworth *et al.,* 2013; Halevy and Head, 2014). Finally, previous workers reported the surface flux. However, as pointed out by other workers, while the

flux is the relevant quantity when computing energy deposition, when computing molecular reaction rates the spherically integrated intensity, or actinic flux, is the more relevant quantity (Madronich, 1987; Kylling *et al.,* 1995). For a particle lying at the planetary surface, fluence below the horizon is blocked by the surface. Therefore, we report instead the integral of the intensity field at the planetary surface over the hemisphere defined by elevations >0 (*i.e.,* that part of the sky not blocked by the planetary surface). We term this quantity the *surface radiance*. For more details, see Ranjan and Sasselov (2017).

3. Methods

In this section, we describe the methods used to calculate the surface UV environment of early Mars. All software associated with this project is available for validation and extension at https://github.com/sukritranjan/ranjanwordsworthsasselov2016.

3.1. Radiative transfer model

We use a multilayer, two-stream approximation to compute the 1-D radiative transfer of UV light through the early martian atmosphere. Our code is based on the radiative transfer model of Ranjan and Sasselov (2017). In brief, we follow the two-stream treatment of Toon *et al.* (1989), and we use Gaussian (single) quadrature to connect the diffuse intensity to the diffuse flux, since Toon *et al.* (1989) found Gaussian quadrature closure to be more reliable than Eddington or hemispheric mean closure at short (solar) wavelengths. We include absorption and scattering due to N_2, CO_2, H_2O, CH_4, O_2, O_3, SO_2, and H_2S. For reasons of numerical stability, we assign a ceiling on the per-layer single-scattering albedo ω_0 of $1-10^{-12}$. Ranjan and Sasselov (2017) included thermal emission from the atmosphere and surface to enable application of our code to situations where planetary UV emission might be important. Early Mars is not such a case, so here we omit these features.

Our model requires the user to specify the partition of the atmosphere into homogeneous layers and provide the temperature, pressure, and composition (gaseous molar concentrations) as a function of altitude. Section 3.2 describes our calculation of these quantities. Our model also requires the user to specify the wavelength bins over which the radiative transfer is to be computed; all spectral parameters are integrated over these wavelength bins by using linear interpolation in conjunction with numerical quadrature. The user also must specify the SZA and albedo. The albedo may be specified as either a fixed value (*e.g.,* Rugheimer *et al.,* 2015) or as a wavelength- and SZA-dependent user-determined mix of the albedos corresponding to different terrestrial physical surface media (new snow, old snow, desert, tundra, ocean).

We take the TOA flux to be the solar flux at 3.9 Ga, computed at 0.1 nm resolution from the model of Claire *et al.* (2012) and scaled to the martian semimajor axis of 1.524 AU. We choose 3.9 Ga for the prebiotically relevant era due to the following: (1) evidence for at least transient liquid water on Mars around this time (Bristow *et al.,* 2015; Grotzinger *et al.,* 2015; Wordsworth, 2016); (2) this post-dates the potentially sterilizing Late Heavy Bombardment (Maher and Stevenson, 1988; Sleep *et al.,* 1989); and (3)

---

[2]This regime is not available on modern Earth or Mars, due to oxic absorption in the former and a thin atmosphere in the latter.

this predates the bulk of the evidence for the earliest terrestrial life (see Ranjan and Sasselov, 2016, and sources therein). If hypothesizing that terrestrial abiogenesis was aided by transfer of prebiotically relevant compounds from Mars (Benner, 2013; Gollihar et al., 2014; Benner and Kim, 2015), it would follow that the synthesis of these molecules and their transfer would have occurred concomitantly with the origin of life on Earth. We note that, unlike the XUV, solar output varies only modestly (within a factor of 2) from 3.5–4.1 Ga in the >180 nm wavelength range unshielded by atmospheric CO_2 or H_2O. Therefore, our results are insensitive to the precise choice of epoch for abiogenesis.

Ranjan and Sasselov (2017) did not include scattering and absorption due to atmospheric particulates. However, clouds were suggested to play a major role in the martian paleoclimate (Forget and Pierrehumbert, 1997; Colaprete and Toon, 2003; Wordsworth et al., 2013). Therefore, we have updated our model to allow the user to emplace CO_2 and H_2O cloud decks of user-specified optical depth (at 500 nm) in the atmosphere. The cloud decks are assumed to uniformly span the atmospheric layers into which they are emplaced. In Section 3.3, we discuss the calculation of the particulate optical parameters (per-particle cross section σ, asymmetry parameter g, and ω_0). We use delta-scaling with Henyey-Greenstein closure (Joseph et al., 1976) to correct for the effects of highly forward-peaked particulate scattering phase functions.

The fundamental output of our code is the surface radiance as a function of wavelength. The surface radiance is the integral of the intensity field at the planetary surface over the unit hemisphere defined by elevations greater than zero, that is, the intensity field integrated over all parts of the sky that are not blocked by the planetary surface. As Ranjan and Sasselov (2017) purported, this is the relevant quantity for calculating reaction rates of molecules at planetary surfaces (as compared to the actinic fluxes for molecules suspended in the atmosphere, see Madronich, 1987). In the two-stream formalism, this quantity is

$$I_{surf} = F_N^{\downarrow}/\mu_1 + F_N^{dir}/\mu_0$$

where $F_N^{\downarrow}$ is the downward diffuse flux at the planetary surface, F_N^{dir} is the direct flux at the planetary surface, and $\mu_0 = \cos(SZA)$ is the cosine of the solar zenith angle. In Gaussian quadrature for the $n=1$ (two-stream) case, $\mu_1 = 1/\sqrt{3}$ (Toon et al., 1989); it can be interpreted as the effective zenith angle for the diffuse flux.

3.2. Atmospheric profile

We assume a CO_2-dominated martian atmosphere at 3.9 Ga. We take the atmosphere to be fully saturated with H_2O. Typical calculations of Noachian climate call for steady- state local surface temperatures of $T_0 \lesssim 273$ K across the planetary surface, and more typically $T_0 \sim 210$–250 K (Forget et al., 2013; Wordsworth et al., 2013). Both 1-D and 3-D calculations of Noachian climate produce global mean surface temperatures of 240 K or less (Forget et al., 2013; Wordsworth et al., 2013; Ramirez et al., 2014). At such cold temperatures, the H_2O saturation pressure is very low, and H_2O is a trace gas in the atmosphere. Therefore, we approximate the thermodynamic properties of

the martian atmosphere by the thermodynamic properties of CO_2. We take $c_p = c_{p,CO_2}$ and $R = R_{CO_2}$, where c_p and R are the heat capacity at constant pressure and the specific gas constant, respectively. We assume the heat capacity to be constant, with $c_p = c_p(T_0)$, where T_0 is the surface temperature. We calculate $c_p = c_{p,CO_2}$ from the Shomate relation, taking the coefficients from the work of Pierrehumbert (2010, p 115). We tested the effects of permitting the heat capacity to vary with temperature and found minimal impact on our results.

Martian paleoclimate models have been proposed that invoke effects like enhanced volcanism (Halevy and Head, 2014) and high H_2 abundance (Ramirez et al., 2014) to argue for global mean temperatures in excess of 273 K. However, these models also require pCO_2 in excess of 1 bar, meaning that H_2O remains a trace atmospheric constituent. Regardless, our results are insensitive to the precise thermal properties of the atmosphere because of the modest variation of the absorption cross sections of the gases in our model with temperature at UV wavelengths.

For a given surface pressure and surface temperature (P_0, T_0), we let the temperature decrease as a dry adiabat until it reaches the CO_2 saturation temperature, at which point it follows the CO_2 saturation curve. We use the empirical saturation curve of Fanale et al. (1982), as in the work of Wordsworth et al. (2013). To avoid the need for a full radiative-convective climate model, which is tangential to our objectives in this paper, we assume a stratosphere starting at 0.1 bar, following the observation of Robinson and Catling (2014) that atmospheres dominated by triatomic gases tend to become optically thin and hence radiatively dominated around that pressure. We follow other workers (e.g. Kasting, 1991; Hu et al., 2012; Halevy and Head, 2014) assuming the stratosphere to be isothermal; we conduct sensitivity studies that demonstrate our results are not sensitive to this assumption.

To calculate the H_2O saturation pressure, we use the empirical formulation of Wagner et al. (1994) via the work of Wagner and Pruß (2002) for the vapor pressure of water overlying a solid reservoir (as would be the case for $T_0 < 273$ K). We assume the atmosphere to be fully saturated in H_2O until the tropopause, and we assume the molar concentration of water in the stratosphere to be equal to its concentration at the tropopause throughout.

Our model requires temperature, pressure, and molar concentrations as functions of altitude. To obtain a mapping between pressure and altitude, we approximate the atmosphere as a series of 1000 layers, each individually isothermal, evenly spanning $P_0 - P_0 \times \exp(-10)$. We then use the equation for an isothermal atmosphere in hydrostatic equilibrium,

$$P(z)/P(z_0) = \exp(-(z - z_0)/H)$$

to calculate the change in altitude across each pressure layer, and sum to obtain a mapping between z and P. Here, P is pressure, z is the altitude of the layer top, z_0 is the altitude of the layer bottom, and $H = kT/(\mu g)$ is the scale height of the layer, with T being the layer temperature, μ the mean molecular weight of the atmospheric layer, and g the acceleration due to martian gravity. We also considered numerically integrating the hydrostatic equilibrium equation,

$$dP/dz = -\rho g$$

where the density $\rho = \mu P/(kT)$ for an ideal gas, directly to obtain $z(P)$. We found this approach to agree within 1%; we consequently elected to use the simpler isothermal partition approach for our calculation. Appendix A presents sample atmospheric profiles derived by using our methods.

3.3. Particulate optical parameters

In this section, we discuss our calculation of the optical parameters (σ, ω_0, and g) associated with interaction of radiation with the CO_2 and H_2O ice particles that constitute clouds.

We approximate the particles as spherical and compute their optical parameters using Mie theory at 0.1 nm resolution, following the treatment outlined by Hansen and Travis (1974). At each wavelength, we compute ω_0, g, and the scattering efficiency Q_s. We numerically integrate these parameters over a log-normal size distribution with effective radius r_{eff} and effective variance v_{eff}, weighted by $\pi r^2 n(r)$, where r is the particle radius and $n(r)$ is the size distribution, and demand a precision of 1% in the distribution-averaged mean values. We obtain the per-particle total extinction cross section by

$$\sigma = (\overline{Q_s}/\overline{\omega_0}) G$$

where $\overline{Q_s}$ is the distribution-averaged mean value of Q_s, $\overline{\omega_0}$ is the distribution-averaged mean value of ω_0, and

$$G = \int_{r_1}^{r_2} \pi r^2 n(r) dr$$

is the "geometric cross-sectional area of particles per unit volume" (Hansen and Travis, 1974) computed at 1 ppm precision. For our numerical integral, we integrated from $r_1 = r_{eff} 10^{-10 v_{eff}}$ to $r_2 = r_{eff} 10^{4 v_{eff}}$; we found $n(r) < 10^{-4}$ beyond these limits.

We take the index of refraction for H_2O ice from the compendium of Warren and Brandt (2008)[3]. We take the index of refraction for CO_2 ice from the compendium given in Pierrehumbert (2010)[4]. This compendium was formed by G. Hansen by subjecting the absorption spectra of Hansen (1997) and Hansen (2005) to Kramers-Kronig analysis to obtain self-consistent spectra of real and imaginary indices of refraction (S. Warren, private communication). We take the index of refraction for martian dust from the work of Wolff et al. (2009)[5]. The data of Wolff et al. (2009) truncate at 263 nm. Measurements of the imaginary index of refraction down to 194 nm are available from the work of Pang and Ajello (1977). We adopt the values of Pang and Ajello (1977) for wavelengths < 263 nm. Zurek (1978) presented a compendia of the real index of refraction of martian dust. His study indicates that the index of refraction changes

by only ~0.1 from ~200 to 263 nm. His values at 263 nm are 0.4 higher than those of Wolff et al. (2009); to avoid a discontinuity, we subtract 0.4 from the real indices of refraction of Zurek (1978).

Figure 1 presents the CO_2 and H_2O ice optical parameters as a function of wavelength for size distributions with $v_{eff} = 0.1$ and $r_{eff} = 1$, 10, 100 microns. Previous work has assumed CO_2 cloud particle sizes to be in the 1–100 μm range (e.g., Forget and Pierrehumbert, 1997). Microphysical modeling by Colaprete and Toon (2003) suggests that primitive martian CO_2 clouds may have been characterized by large particle sizes, as high as $r_{eff} = 100$ μm. The optical properties of CO_2 and H_2O ice particles for $r_{eff} \geq 10$ μm are insensitive to r_{eff}; we attribute this to size parameter $x = 2\pi r_{eff}/\lambda$ being large in this regime, meaning such particles approach the large-particle limit ($x > 12$ for $r_{eff} \geq 10$ μm and $\lambda \leq 500$ nm). For wavelengths satisfying $195 < \lambda < 500$ nm, CO_2 and H_2O ice are characterized by $\omega_0 \approx 1$. This means that CO_2 and H_2O clouds do not significantly absorb at wavelengths unshielded by H_2O (<198 nm) or CO_2 (<204 nm). By contrast, dust absorbs across 100–500 nm, meaning dust particles can supply absorption at wavelengths not shielded by CO_2 or H_2O.

3.4. Action spectra and calculation of dose rates

To quantify the impact of different surface UV radiation environments on prebiotic chemistry, we follow the approach of Cockell (1999), Rontó et al. (2003), and Rugheimer et al. (2015) in computing biologically effective dose rates. Specifically, we compute

$$D = \left(\int_{\lambda_0}^{\lambda_1} d\lambda \mathcal{A}(\lambda) I_{surf}(\lambda) \right)$$

where $\mathcal{A}(\lambda)$ is an action spectrum, λ_0 and λ_1 are the limits over which $\mathcal{A}(\lambda)$ is defined, and $I_{surf}(\lambda)$ is the UV surface radiance. An action spectrum parametrizes the relative impact of radiation on a given photoprocess as a function of wavelength, with a higher value of $\mathcal{A}$ meaning that a higher fraction of the incident photons are being used in the photoprocess. Hence, D is proportional to the reaction rate of a given photoprocess for a single molecule at the surface of a planet.

As D is a relative measure of reaction rate, a normalization is required to assign a physical interpretation to its value. In this paper, we report

$$\overline{D} = D/D_{\oplus}$$

where $D_{\oplus}$ is the dose rate on 3.9 Ga Earth. The atmospheric model for 3.9 Ga Earth is taken from the work of Rugheimer et al. (2015), who used a 1-D coupled climate-photochemistry model to compute the atmospheric profile (T, P, composition) for Earth at 3.9 Ga, assuming modern abiotic outgassing rates and a background atmosphere of 0.9 bar N_2, 0.1 bar CO_2, with SZA = 60° and $A = 0.2$. Consequently, $\overline{D} > 1$ means that the photoprocess is proceeding faster on the martian surface under the specified atmosphere than it would on the surface of the Rugheimer et al. (2015) fiducial Earth. Note that this normalization is different from what Ranjan and Sasselov (2017) chose, because here we

---

[3]Accessed via http://www.atmos.washington.edu/ice_optical_constants

[4]Accessed via http://geosci.uchicago.edu/~rtp1/PrinciplesPlanetary Climate/Data/WorkbookDatasets/Chapter5Data/co2i4a.rfi.txt

[5]Accessed via http://spacescience.arc.nasa.gov/mars-climate-modeling-group/documents/ Dust_Refractive_Indicies.txt
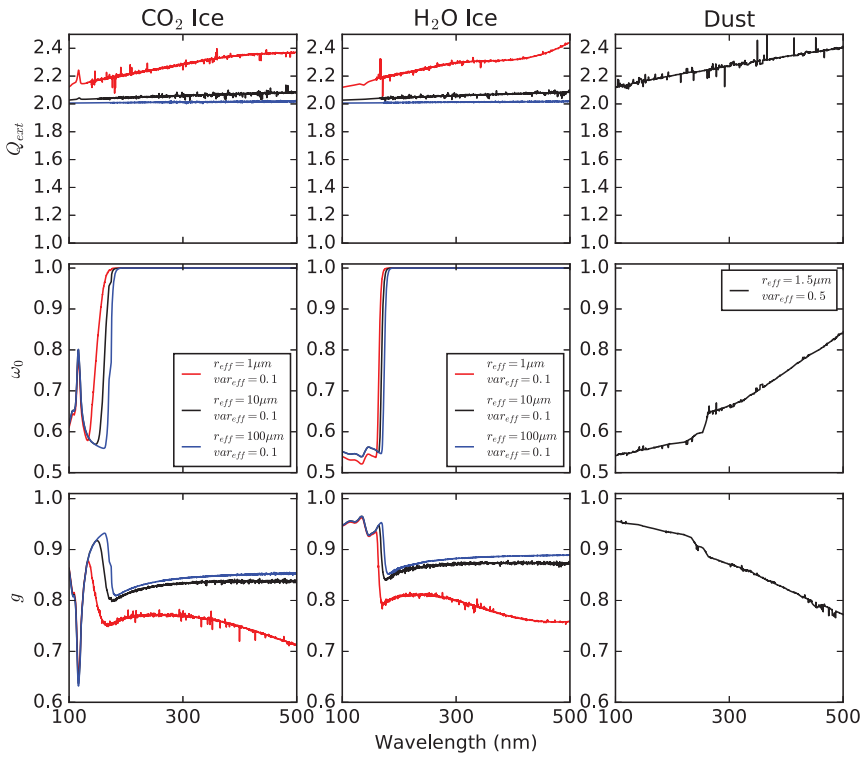
FIG. 1. Scattering efficiency Q_{ext}, single-scattering albedo ω_0, and asymmetry parameter g as a function of wavelength for CO_2 ice, H_2O ice, and modern martian dust, integrated over the specified log-normal size distributions.

are trying to assess how Mars compares to Earth as a venue for prebiotic chemistry.

Previous workers have used action spectra of UV stress on modern biology (*e.g.,* the DNA inactivation action spectrum) (Cockell, 2000, 2002; Cnossen *et al.,* 2007; Rugheimer *et al.,* 2015) as a gauge of the level of stress imposed by UV fluence on the prebiotic environment. However, these action spectra are based on modern life. Modern organisms have evolved sophisticated methods with which to tolerate environmental stresses, including UV exposure, that would not have been available to the first life. Further, this approach presupposes that UV light is solely a stressor and ignores its potential role as a eustressor for abiogenesis. In this work, we follow the reasoning of Ranjan and Sasselov (2017) in formulating action spectra that correspond to simple photoreactions that are expected to have played major roles in prebiotic chemistry. We consider two reactions: a stressor process, to capture the stress UV light places on nascent biology, and an eustressor process, to capture the role of UV light in promoting prebiotic chemistry. A detailed description of these processes and their corresponding action spectra was given by Ranjan and Sasselov (2017); a brief outline is presented below.

3.4.1. Stressor process: cleavage of N-glycosidic bond of UMP.

For our stressor process, we chose the cleavage of the N-glycosidic bond in the RNA monomer uridine monophosphate (UMP). UV radiation can cleave the N-glycosidic bond that joins the sugar to the nucleobase (Gurzadyan and Görner, 1994), irreversibly destroying this molecule. Hence, this process represents a stressor to abiogenesis.

The action spectrum is equal to the product of the absorption spectrum (fraction of incident photons absorbed) and the quantum yield (QY, fraction of absorbed photons that lead to the photoreaction) curve. We take our UMP absorption

spectrum from the work of Voet *et al.* (1963) (pH = 7.6). Detailed spectral measurements of the QY of glycosidic bond cleavage, to date, have not been obtained. However, Gurzadyan and Görner (1994) found the QY of N-glycosidic bond cleavage in UMP in neutral aqueous solution saturated with Ar (*i.e.,* anoxic) to be 4.3×10^{-3} at 193 nm and $(2-3) \times 10^{-5}$ for 254 nm. We therefore represent the QY curve as a step function with value 4.3×10^{-3} for $\lambda \leq \lambda_0$ and 2.5×10^{-5} for $\lambda > \lambda_0$. We consider λ_0 values of 193 and 254 nm, corresponding to the empirical limits from the work of Gurzadyan and Görner (1994). We also consider $\lambda_0 = 230$ nm, which corresponds to the end of the broad absorption feature centered near 260 nm, corresponding to the $\pi–\pi^*$ transition and also to the transition to irreversible decomposition suggested by Sinsheimer and Hastings (1949). As shorthand, we refer to this photoprocess under the assumption that $\lambda_0 = X$ nm by UMP-X. Figure 2 presents these action spectra.

The absorption spectra of the other RNA monomers are structurally similar to UMP (Voet *et al.,* 1963), and the QY of N-glycosidic bond cleavage in adenosine monophosphate (AMP) increases at short wavelengths as does UMP's (Gurzadyan and Görner, 1994), which leads us to argue that action spectra for N-glycosidic bond cleavage of the other RNA monomers should be broadly similar to that for UMP. Therefore, results derived by using the action spectrum for UMP N-glycosidic bond cleavage should be broadly applicable to the other RNA monomers; if a UV environment is destructive for UMP, it should be bad for the other RNA monomers and, hence, for abiogenesis in the RNA world hypothesis as well.

3.4.2. Eustressor process: production of aquated electrons from photoionization of cyanocuprate.

For our eustressor process, we choose the production of aquated electrons from the irradiation of a tricyanocuprate
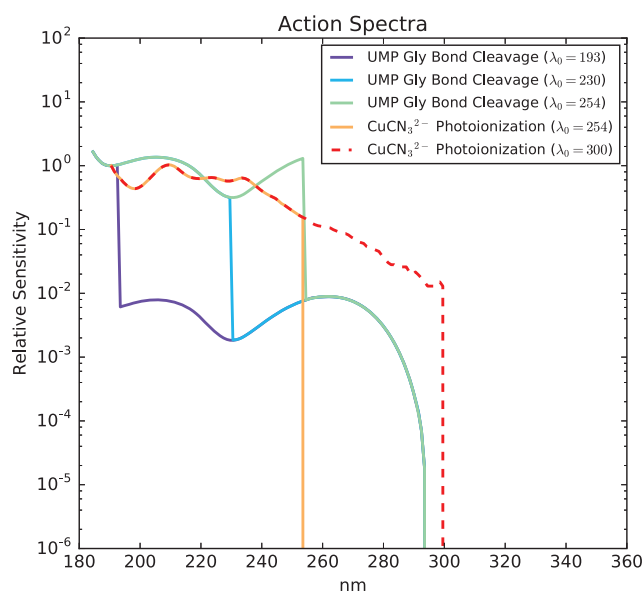
FIG. 2. Action spectra for photolysis of UMP-λ_0 and photoionization of CuCN3-λ_0, assuming a step-function form to the QY for both processes with step at λ_0. The spectra are arbitrarily normalized to 1 at 190 nm.

(CuCN$_3^{2-}$) complex. We chose this process because it underlies the selective 2- and 3-carbon sugar (glycolaldehyde and glyceraldehyde) synthesis pathway of Ritson and Sutherland (2012), which is the best candidate proposed so far for a selective prebiotic synthesis of these sugars. These sugars are required for the synthesis of RNA and, hence, abiogenesis in the RNA world hypothesis. This process is also important to the prebiotic reaction network of Patel *et al.* (2015). More generally, aquated electrons are useful for a broad range of reductive prebiotic chemistry, for example, the reduction of nitriles to amines, aldehydes to hydroxyls, and hydroxyls to alkyls[6]. Therefore, this process represents a eustressor to abiogenesis. While other UV-sensitive processes conducive to abiogenesis doubtless exist, we argue this process is of particular interest because of its unique role in the most promising plausibly prebiotic pathways to the RNA monomers.

We again form the action spectrum by multiplying the absorption spectrum and the QY curve. We take the cyanocuprate absorption spectrum from the work of Magnani (2015), via Ranjan and Sasselov (2016). The spectral QY of aquated electron production from cyanocuprate irradiation is not known. However, Horváth *et al.* (1984) measured a QY of 0.06 for this process at 254 nm. Following the hypothesis of Ritson and Sutherland (2012), which asserts that photoionization of the complex drives aquated electron production, we assume the QY to be characterized by a step function with value 0.06 for $\lambda \leq \lambda_0$ and 0 otherwise. We empirically know $\lambda_0 \geq 254$ nm. To explore a range of λ_0, we consider $\lambda_0 = 254$ nm and $\lambda_0 = 300$ nm. As shorthand, we refer to this photoprocess under the assumption that $\lambda_0 = Y$ nm by CuCN3-Y. Figure 2 presents these action spectra.
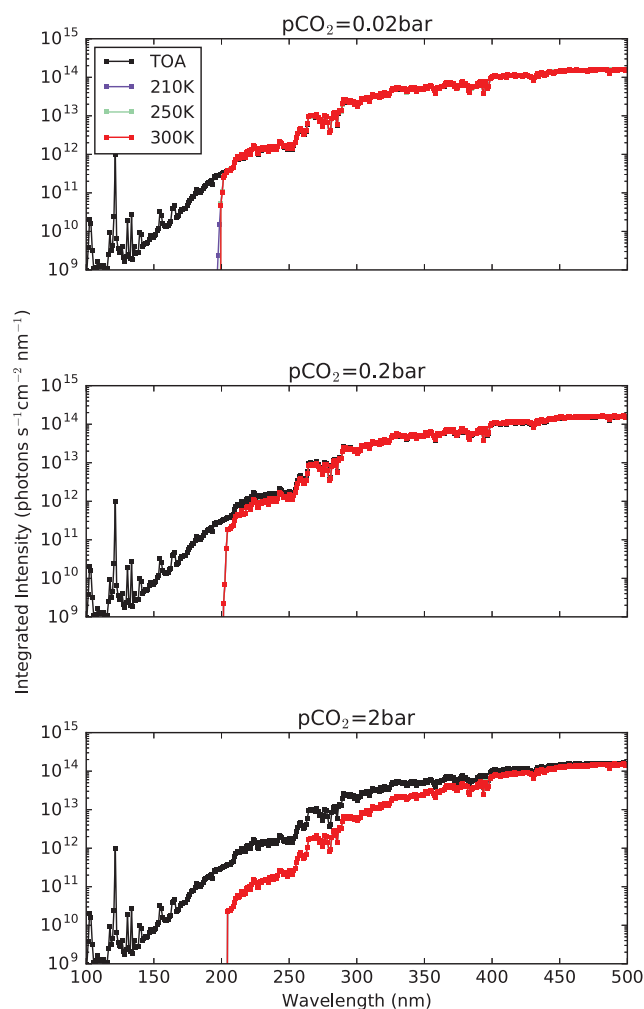
---

[6]J. Szostak, private communication, 2/5/16.

FIG. 3. Surface radiance as a function of wavelength for varying pCO$_2$ and T_0, for SZA = 0 and albedo corresponding to desert. Also plotted for scale is the TOA solar flux. The surface radiance is insensitive to atmospheric and surface temperature. Color images available online at www.liebertpub.com/ast

Action spectra typically encode information about relative, not absolute, reaction rates. Consequently, they are generally arbitrarily normalized to 1 at some wavelength (see, *e.g.,* Cockell, 1999, and Rugheimer *et al.,* 2015). We normalize these spectra to 1 at 190 nm.

4. Results

4.1. Clear-sky H$_2$O-CO$_2$ atmospheres

We evaluated the UV surface radiance for a range of (pCO$_2$, T_0) for pure H$_2$O-CO$_2$ atmospheres in the clear-sky case (no clouds, dust, or other particulates). We considered pCO$_2$ = 0.02–2 bar, corresponding to the range of surface pressure for which Wordsworth *et al.* (2013) reported at least transient local temperatures above 273 K, and T_0 = 210–300 K. We took an SZA of 0, corresponding to noon at equatorial latitudes. We took the surface albedo to correspond to desert (diffuse albedo of 0.22); we adopted this albedo because young Mars is thought to have been dry and desertlike in conventional climate models. Modern Mars
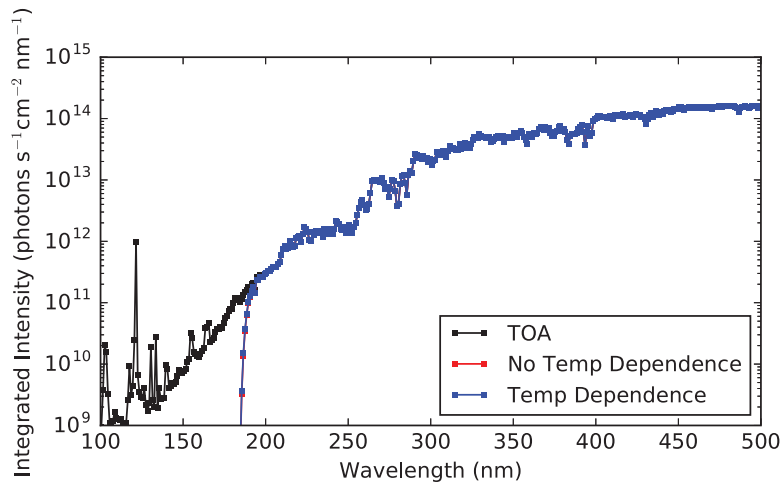
FIG. 4. Surface radiance as a function of wavelength for $pCO_2 = 2 \times 10^{-5}$ bar, $T_0 = 200$ K, SZA $= 0$, A corresponding to desert, with and without temperature dependence of the CO_2 cross sections included. Also plotted for scale is the TOA solar flux. The surface radiance is insensitive to inclusion of temperature dependence of the CO_2 cross sections, even for very low pCO_2.

has a UV albedo an order of magnitude lower (Fox *et al.,* 1997), likely due to the formation of UV-absorbing metal oxides on the planet's basaltic surface over geological time; sensitivity tests indicate our results are robust to choices of surface albedo down to $A \sim 0.02$. Taken together, variations in surface albedo and SZA can drive variations in the spectral surface radiance of up to a factor of ~ 20 and overall variations in prebiotically relevant reaction rates of a factor of $\gtrsim 10$ (Ranjan and Sasselov, 2017). These surface radiances are shown in Fig. 3.

In the scattering regime ($\lambda > 204$ nm), our surface radiances fall off only slowly with pCO_2. This is a consequence of random walk statistics in the context of multiple scattering: transmission through purely scattering media go as $1/\tau$ (see, *e.g.,* Bohren, 1987, for a discussion with application to clouds). This result stands in contrast to the calculations of Cnossen *et al.* (2007) and Rontó *et al.* (2003), who ignore multiple scattering in their radiative transfer treatments, and illustrates the importance of self-consistently including this phenomenon when considering dense, highly scattering atmospheres.

We find our surface radiance calculations to be insensitive to T_0. This is because (1) the total atmospheric column is set by P_0 and independent of T_0; (2) the rapid increase of CO_2 cross sections for $\lambda < 204$ nm, which means that the atmosphere rapidly becomes optically thick in the UV; and (3) increased water-vapor abundance with increasing T_0 does not drive an increase in opacity, because water-vapor absorption is degenerate with CO_2 absorption in the UV (Ranjan and Sasselov, 2017).

We considered the hypothesis that including the effect of variations in CO_2 cross section with temperature might impact our results. We followed the approach of Hu *et al.* (2012) in interpolating between cold (~ 195 K) and room-temperature data sets for CO_2 absorption to estimate the effects of temperature dependence on CO_2 cross section. We used the data set of Stark *et al.* (2007) from 106.5 to 118.7 nm, Yoshino *et al.* (1996) from 118.7 to 163 nm, and Parkinson *et al.* (2003) from 163 to 192.5 nm. We did not find cold-temperature cross sections for CO_2 at longer wavelengths. We found our results were not altered by including temperature dependence of CO_2 cross sections for $pCO_2 = 0.02$–2 bar, because the CO_2 UV absorption is al-

ready saturated by 192.5 nm, where our temperature dependence kicks in. We considered lower values of $pCO_2 = 2 \times 10^{-3}$ to 2×10^{-5} bar (below present atmospheric level), where the CO_2 absorption does not saturate until wavelengths shorter than 192.5 nm. Even in the low pCO_2 case, including temperature dependence only changed the onset of CO_2 absorption saturation by 1–2 nm. We attribute this to the rapidity of the rise in CO_2 absorption cross section with decreasing wavelength for $\lambda \lesssim 204$ nm. We conclude that even including the effects of temperature on CO_2 UV cross section, the UV surface fluence is insensitive to T_0. We consequently elected to ignore the temperature dependence of CO_2 cross sections in the remainder of this study.

Figure 4 presents the surface radiances in the $pCO_2 = 2 \times 10^{-5}$ bar cases, calculated for SZA $= 0$, A corresponding to desert, and $T_0 = T_{eq} \approx 200$ K, with and without CO_2 cross sections included. Such low atmospheric pressures have been suggested based on atmospheric escape arguments (Tian *et al.,* 2009), followed by a buildup of the atmosphere after escape rates subsided with shortwave solar output. In such a case, aqueous prebiotic chemistry could only have proceeded in environments kept warm by nonclimatological means, for example, geothermal reservoirs. Even for such low pCO_2, EUV fluence shortward of 185 nm is shielded out by atmospheric CO_2.

4.2. Effect of CO_2 and H_2O clouds

We considered the effect of CO_2 and H_2O clouds in a CO_2-H_2O atmosphere. Such clouds have been detected on modern Mars (see, *e.g.,* Vincendon *et al.,* 2011), and GCM (General Circulation Model) results suggest they should have been present on early Mars as well (Wordsworth *et al.,* 2013). Figure 5 presents the UV surface fluence for a 0.02 bar CO_2-H_2O atmosphere with H_2O and CO_2 cloud decks of varying optical depths emplaced in the atmosphere. This low surface pressure is chosen in order to isolate the effects of the clouds as opposed to atmospheric CO_2. The surface albedo corresponds to desert, and SZA $= 0$. The optical depths are specified at 500 nm. The H_2O and CO_2 cloud decks are emplaced from 3 to 4 km and 20 to 21 km of altitude, respectively, corresponding approximately to
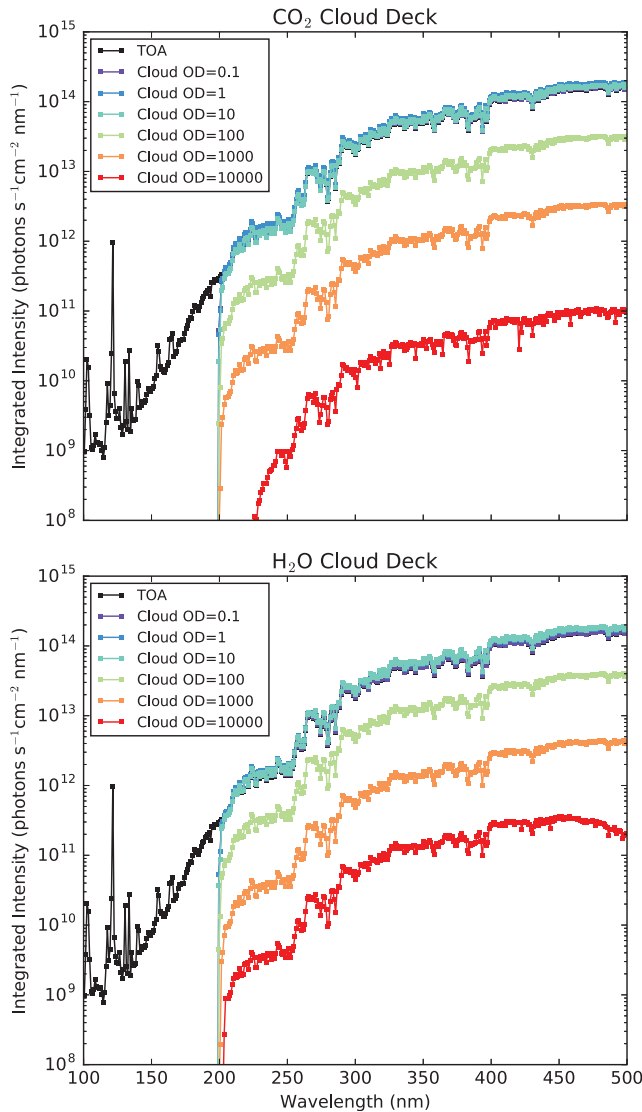
FIG. 5. Surface radiance as a function of wavelength for $pCO_2 = 0.02$ bar, $T_0 = 250$ K, SZA = 0, A corresponding to desert, and CO_2 and H_2O cloud decks of varying thicknesses inserted from 20 to 21 and 3 to 4 km, respectively. Also plotted for scale is the TOA solar flux.

the altitudes of peak cloud formation identified by Wordsworth *et al.* (2013). For both types of clouds, we varied the cloud deck altitudes between 0.5 and 60.5 km and found the surface fluence to be insensitive to the cloud deck altitude. We also experimented with partitioning the clouds into two decks and found the surface fluence to be insensitive to the partition.

CO_2 and H_2O ice clouds have similar impact on the surface fluence. This is because both types of ice have similar optical parameters for $195 < \lambda < 500$ nm and $r_{eff} \geq 1$ μm. The $\lambda < 195$ nm regime, where they have different optical parameters, is shielded out by gaseous CO_2 absorption.

CO_2 and H_2O ice particles are pure scatterers for $195 < \lambda < 500$ nm and $r_{eff} \geq 1$ μm. Consequently, it is unsurprising that surface fluence falls off only slowly with increasing optical depth. In fact, the transmission of a purely scattering cloud layer varies as $\sim 1/\tau^*$, where τ^* is the delta-

scaled optical depth of the cloud layer (Bohren, 1987). This is a consequence of the random-walk nature of radiative transfer in the optically thick, purely scattering limit.

The particle size r_{eff} can have an impact on surface radiance. For $r_{eff} = 1$ μm, the surface fluence at 500 nm is $\sim 40\%$ lower compared to $r_{eff} = 100$ μm (A corresponding to desert, SZA = 0). This is because as r_{eff} decreases in this regime, so does g, meaning that the rescaled optical depth in the delta-scaling formalism $\tau^* = \tau \times (1 - g^2)$ is higher for small particles than large particles.

Suppressing surface radiance to 10% or less of TOA flux requires cloud optical depths of $\gtrsim 100$. This is comparable to the optical depth of a terrestrial thunderstorm (Mayer *et al.*, 1998). We can compute the mass column of ice particles required to achieve this optical depth by

$$u = \left(\frac{\tau}{\pi r^2 Q_{ext}}\right)\left(\frac{4\pi}{3}r^3\rho\right)$$

where ρ is the mass density of the ice, r is the ice particle radius, τ is the cloud optical depth, and Q_{ext} is the extinction efficiency. For CO_2 ice, $\rho = 1.5$ g/cm^3[7], $r = 10$ μm, and approximating $Q_{ext} = 2$, we find $\tau = 100$ corresponds to $u = 1$ kg/m^2. Wordsworth *et al.* (2013) found in their 3-D simulation CO_2 ice columns of up to 0.6 kg/m^2 in patches, suggesting CO_2 clouds may have significantly affected the surface UV environment. For water ice, taking $\rho = 0.92$ g/cm^3 (Miller, 2009), $r = 10$ μm, and approximating $Q_{ext} \approx 2$, we find that $\tau = 100$ corresponds to $u = 6 \times 10^{-1}$ kg/m^2. By contrast, Wordsworth *et al.* (2013) found expected ice columns of $\lesssim 2 \times 10^{-3}$ kg/m^2. Consequently, barring a mechanism that can increase the H_2O cloud levels above that considered by Wordsworth *et al.* (2013), H_2O ice clouds by themselves are unlikely to significantly alter the surface radiance environment on early Mars.

4.3. Effect of elevated levels of volcanogenic gases

So far, we have considered pure CO_2-H_2O atmospheres. However, other gases may have been present in the early martian atmosphere. In particular, Mars at ~ 3.9 Ga was characterized by volcanic activity, which emplaced features like the Tharsis igneous province (Halevy and Head, 2014). Such volcanism could have injected elevated levels of volcanogenic gases like SO_2 and H_2S into the atmosphere. SO_2 and H_2S are also strong and broad UV absorbers, and at elevated levels they can completely reshape the surface UV environment (Ranjan and Sasselov, 2017). Consequently, we consider the impact of elevated levels of SO_2 and H_2S on the surface UV environment.

We consider SO_2 levels up to 2×10^{-5} bar. For scale, Halevy and Head (2014) computed that an SO_2 level of 1×10^{-5} bar in a 1 bar CO_2-dominated atmosphere requires volcanic outgassing at 100× the current terrestrial outgassing. Figure 6 presents the surface radiance for varying pSO_2 and $pCO_2 = 0.02$–2 bar (SZA = 0, A corresponding to desert, and $T_0 = 250$ K).

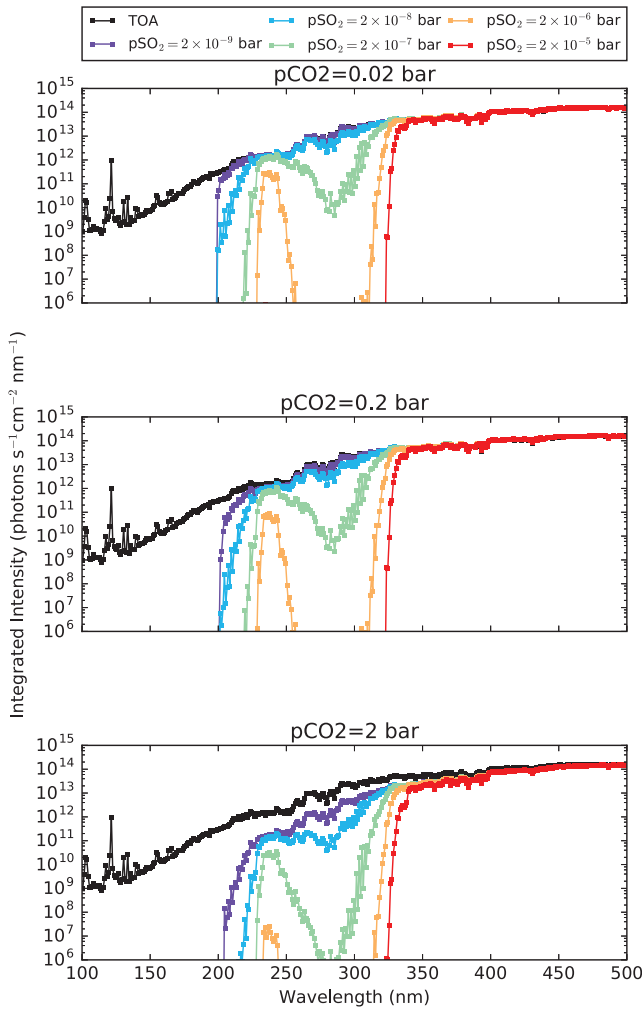[7]http://terpconnect.umd.edu/~choi/MSDS/Airgas/CARBON%20DIOXIDE.pdf

FIG. 6. Surface radiance as a function of wavelength for $T_0 = 250\,K$, $SZA = 0$, A corresponding to desert, $pCO_2 = 0.02$–2 bar, and $pSO_2 = 2 \times 10^{-9}$ to 2×10^{-5} bar. Also plotted for scale is the TOA solar flux.
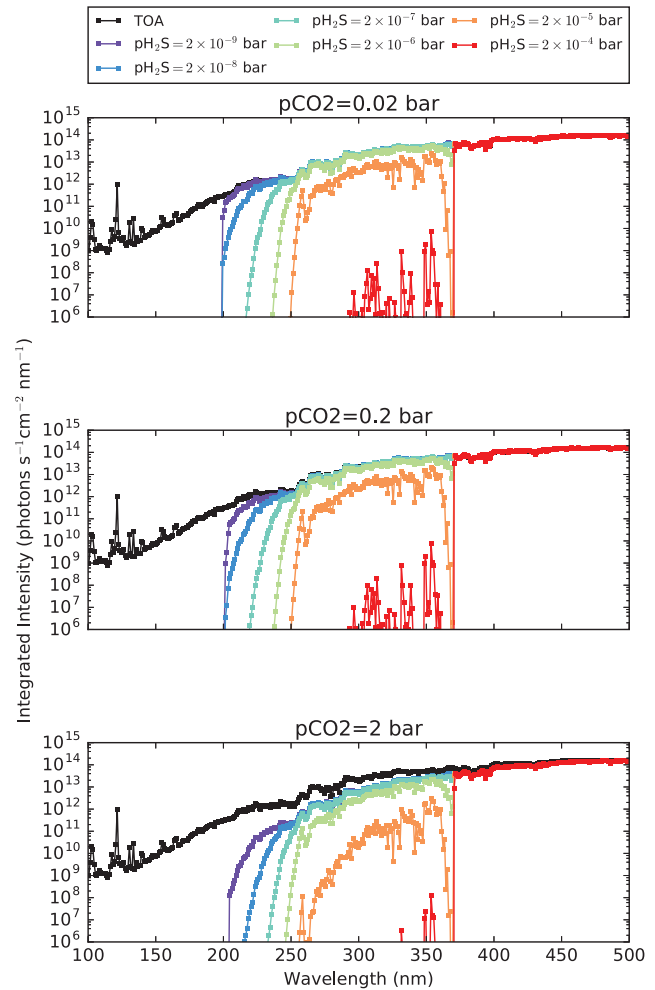
FIG. 7. Surface radiance as a function of wavelength for $T_0 = 250\,K$, $SZA = 0$, A corresponding to desert, $pCO_2 = 0.02$–2 bar, and $pH_2S = 2 \times 10^{-9}$ to 2×10^{-4} bar. Also plotted for scale is the TOA solar flux.

Note that for the same pSO_2, the surface radiance varies as a function of pCO_2. This is because at high pCO_2, the scattering optical depth of the atmosphere exceeds unity. In such a regime, the impact of trace absorbers is amplified due to higher effective path length caused by multiple scattering events (Bohren, 1987). This effect has been seen in studies of UV transmittance through thick clouds on Earth as well (Mayer *et al.*, 1998). Consequently, the surface UV environment is a feature of both pCO_2 and pSO_2. For $pSO_2 \geq \times 10^{-5}$ bar, UV fluence < 330 nm is strongly suppressed.

H_2S is also a major volcanogenic gas that may have been emitted at rates greater than or equal to SO_2 on young Mars, based on studies of the oxidation state of martian basalts (Herd *et al.*, 2002; Halevy *et al.*, 2007). While Halevy and Head (2014) did not calculate the H_2S abundance as a function of volcanic outgassing, the calculations of Hu *et al.* (2013) ($T_0 = 288\,K$, modern solar irradiance) suggest that $pH_2S > pSO_2$ in a CO_2-dominated atmosphere. Consequently, we also consider the impact of elevated levels of H_2S, up to $pH_2S = 2 \times 10^{-4}$ bar in atmospheres with $pCO_2 = 0.02$–2 bar. Figure 7 presents the surface radiance

calculated over this range of atmospheres ($SZA = 0$, A corresponding to desert, and $T_0 = 250\,K$). For $pH_2S \geq \times 10^{-4}$ bar, UV fluence < 370 nm is strongly suppressed.

Scattering due to thick cloud decks can also enhance absorption by trace pSO_2 and pH_2S. For $pSO_2 = 2 \times 10^{-7}$ bar and $pCO_2 = 0.02$ bar[8] [$SZA = 0$, A corresponding to new snow (near 1), $T_0 = 250\,K$, $r_{eff} = 10\,\mu m$], inclusion of CO_2 clouds with optical depth of 1000 amplifies attenuation by a factor of 10 at 236.5 nm (optically thin in SO_2 absorption) and by a factor of 10^5 at 281.5 nm (optically thick in SO_2 absorption) compared to what one would calculate by multiplying the transmission from the SO_2 and cloud deck individually. This effect is weaker for low-albedo cases, because there are fewer passes of radiation through the atmosphere due to bouncing between the surface and cloud deck. This nonlinear variance in transmission due to

---

[8]At $pCO_2 = 0.02$ bar, the gaseous scattering optical depth is less than unity for wavelengths longer than 204 nm, meaning that we can attribute this amplification primarily to the cloud deck (as opposed to gaseous scattering).

multiple scattering effects illustrates the need to specify surface albedo, cloud thickness, and absorber level when calculating surface radiances. Figures 8 and 9 present the surface radiance at the base of a $pCO_2 = 0.02$ bar atmosphere with varying levels of SO_2 and H_2S, respectively, with CO_2 cloud decks of optical depths 1–1000 emplaced from 20 to 21 km (SZA = 0, A corresponding to desert, $T_0 = 250$ K, $r_{eff} = 10$ μm).

4.4. Effect of dust

The atmosphere of modern Mars is dusty, with typical dust optical depths varying from $\tau_d \sim 0.2$ to 2 at solar wavelengths (Smith *et al.,* 2002; Lemmon *et al.,* 2015), with the higher values achieved during global dust storms. Mars' dryness contributes to its dustiness, through the availability of desiccated surface to supply dust and the lack of a hydrologic cycle to quickly scrub it from the atmosphere. If one assumes that Mars was similarly dry in the past, dust levels in the martian atmosphere may have been significant.
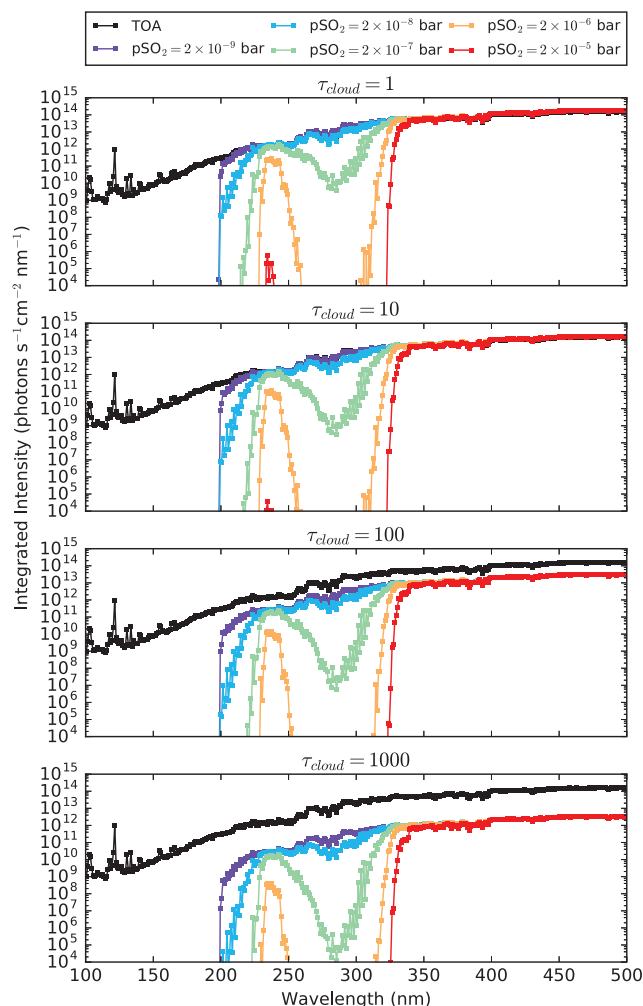
FIG. 8. Surface radiance as a function of wavelength for $T_0 = 250$ K, SZA = 0, A corresponding to desert, $pCO_2 = 0.02$ bar, $pSO_2 = 2 \times 10^{-9}$ to 2×10^{-5} bar, and CO_2 cloud decks of varying optical thickness emplaced from 20 to 21 km altitude. Also plotted for scale is the TOA solar flux.
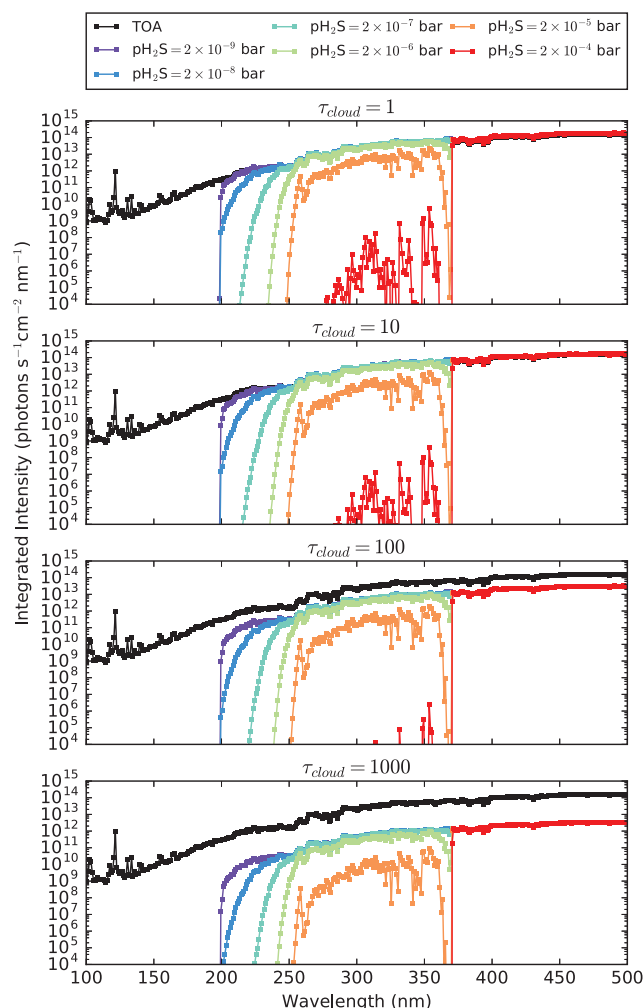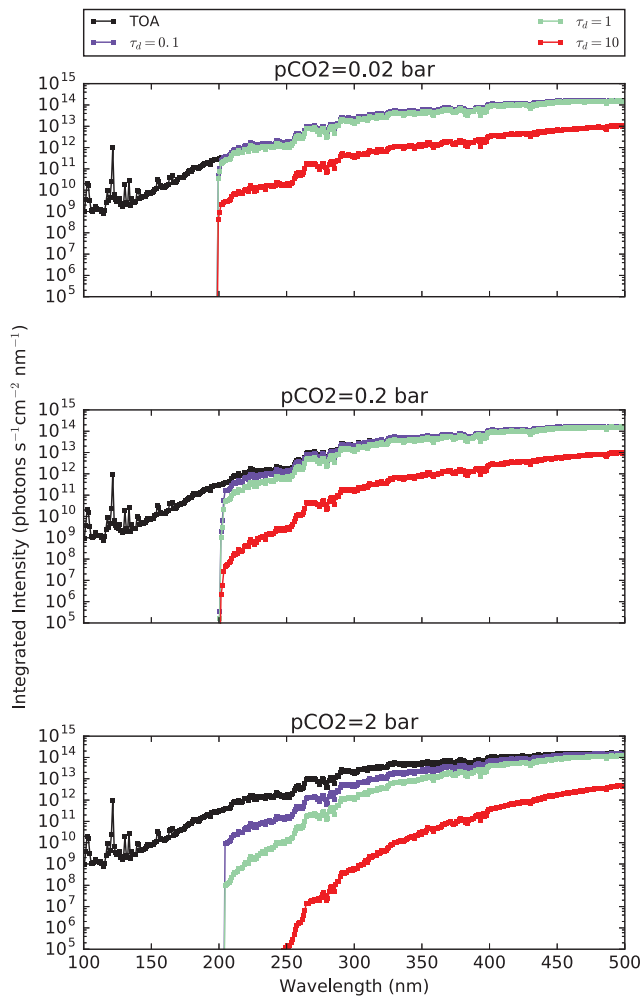

FIG. 9. Surface radiance as a function of wavelength for $T_0 = 250$ K, SZA = 0, A corresponding to desert, $pCO_2 = 0.02$ bar, $pH_2S = 2 \times 10^{-9}$ to 2×10^{-4} bar, and CO_2 cloud decks of varying optical thickness emplaced from 20 to 21 km altitude. Also plotted for scale is the TOA solar flux.

We may speculate that, if the atmosphere were thicker, it could have hosted even more dust than the modern martian atmosphere due to slower sedimentation times. However, detailed study of atmospheric dust dynamics, including analysis of how dust lofting scales with pCO_2, is required to constrain this possibility. Dust absorbs at UV wavelengths (see Fig. 1), so dust could play a role similar to volcanogenic gases in scrubbing UV radiation from the UV surface environment.

We explored the impact of including dust in our calculation of surface UV fluence. We assumed that, similar to modern Mars, the dust followed an exponential profile with scale height $H_d = 11$ km, similar to the atmospheric pressure scale height (Hoekzema *et al.,* 2010; Mishra *et al.,* 2016). For surface temperatures (and hence scale heights) comparable to modern Mars, this corresponds to the assumption by previous workers that the dust mixing ratio is constant in the lower atmosphere (Forget *et al.,* 1999). Then, the dust optical depth across each atmospheric layer of width Δz is

$$C \exp[-z/H_d]$$

where z is the altitude of the layer center. The parameter

$$C = \tau_d(\exp[\Delta z/(2H_d)])(1 - \exp[-\Delta z/H_d])$$

is chosen such that the column-integrated dust optical depth is τ_d.

Figure 10 presents the surface radiance for varying τ_d and $pCO_2 = 0.02$–2 bar (SZA = 0, A corresponding to desert, and $T_0 = 250$ K). As for SO_2 and H_2S, highly scattering atmospheres amplify the impact of trace absorbers. $\tau_d = 1$ only marginally suppresses UV fluence for $pCO_2 = 0.02$ bar, but for $pCO_2 = 2$ bar shortwave fluence is suppressed due to enhanced Rayleigh scattering. In the absence of scattering amplification, $\tau_d \gtrsim 10$ is required to strongly suppress UV fluence.

Figure 11 presents the surface radiance at the base of a $pCO_2 = 0.02$ bar atmosphere with varying τ_d, with CO_2 cloud decks of optical depths 1–1000 emplaced from 20 to 21 km (SZA = 0, A corresponding to desert, $T_0 = 250$ K, $r_{eff} = 10$
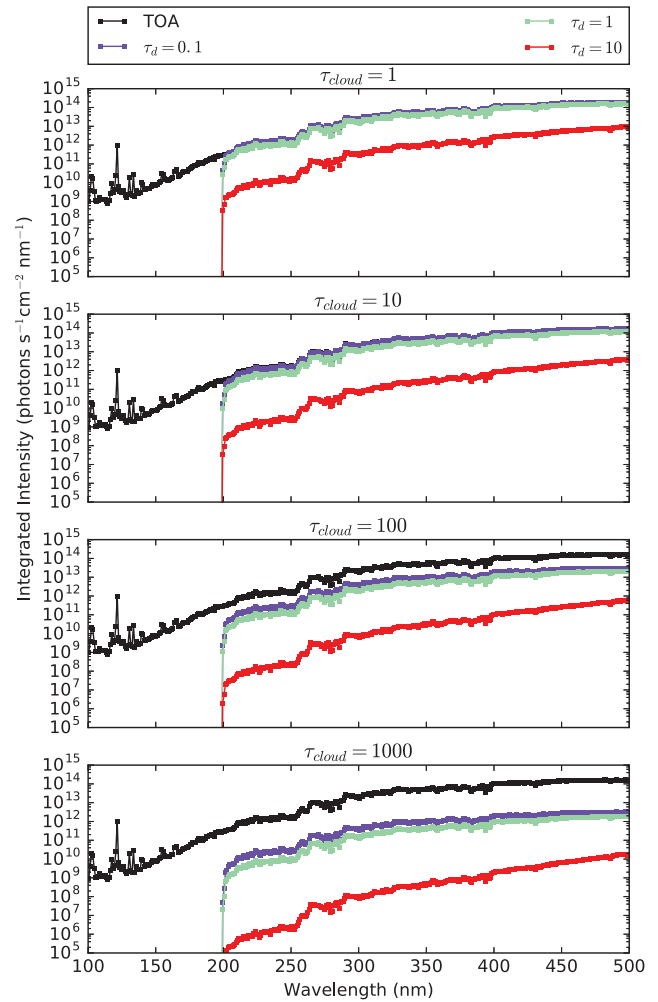

FIG. 10. Surface radiance as a function of wavelength for $T_0 = 250$ K, SZA = 0, A corresponding to desert, $pCO_2 = 0.02$–2 bar, and $\tau_d = 0.1$–10. Also plotted for scale is the TOA solar flux.

FIG. 11. Surface radiance as a function of wavelength for $T_0 = 250$ K, SZA = 0, A corresponding to desert, $pCO_2 = 0.02$ bar, $\tau_d = 0.1$–10, and CO_2 cloud decks of varying optical thickness emplaced from 20 to 21 km altitude. Also plotted for scale is the TOA solar flux.

μm). The impact of a cloud deck is less than the impact of increasing overall atmospheric pressure, because of the limited column of absorber contained within the cloud itself. If the cloud deck is extended, then the surface fluence is reduced (for the same total cloud and dust optical depth).

5. Discussion

5.1. CO_2-H_2O atmosphere

Normative CO_2-H_2O climate models predict the steady-state early martian climate to have been cold, with global mean temperatures below freezing (Forget *et al.,* 2013; Wordsworth *et al.,* 2013, 2015). In this scenario, aqueous prebiotic chemistry would proceed in meltwater pools, which could have occurred transiently during midday due to the diurnal cycle, during summer throughout a seasonal cycle, or a combination of both. Aqueous prebiotic chemistry could also have proceeded in geothermally heated pools, which may have been abundant during the more volcanically active Noachian.
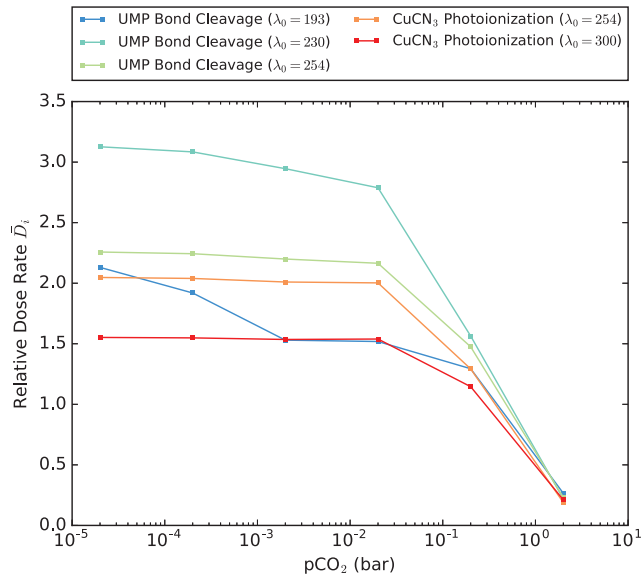
FIG. 12. UV dose rates $\overline{D_i}$ for clear-sky CO_2-H_2O atmospheres as a function of pCO_2 ($T_0 = 250$ K, SZA = 0, A corresponding to desert).

FIG. 13. UV dose rates $\overline{D_i}$ for CO_2-H_2O atmospheres with a CO_2 cloud deck emplaced from 20 to 21 km altitude, as a function of cloud deck optical depth ($T_0 = 250$ K, $pCO_2 = 0.02$ bar, SZA = 0, A corresponding to desert).

Figure 12 presents the dose rates $\overline{D_i}$ corresponding to irradiation of prebiotically relevant molecules through a clear-sky CO_2-H_2O atmosphere with SZA = 0 and A corresponding to desert. The dose rates $\overline{D_i}$ decline by only an order of magnitude across 5 orders of magnitude of $pCO_2 \leq 2$ bar, meaning that the prebiotic photochemistry dose rates are only weakly sensitive to pCO_2 across this range. $\overline{D_i}$ is within an order of magnitude of unity across this range, meaning that the martian dose rates are comparable to the terrestrial rates. This is consistent with the results of Cockell (2000), who found that UV stress as measured by DNA damage was comparable for 3.5 Ga Earth and Mars.

However, the sky was not necessarily clear during this epoch. In fact, formation of H_2O and CO_2 clouds is expected based on GCM studies (Wordsworth *et al.*, 2013). Thick (though patchy) CO_2 cloud decks in particular are expected for thick CO_2 atmospheres. Figure 13 presents the dose rates $\overline{D_i}$ as a function of CO_2 cloud optical depth for $pCO_2 = 0.02$ bar, SZA = 0, and A corresponding to desert. As we might expect from Fig. 5, the dose rate drops off only modestly with τ_{cloud}. $\tau_{\text{cloud}} \gtrsim 1000$ is required to suppress dose rates by more than an order of magnitude. For $r_{\text{eff}} = 10$ μm, this corresponds to 20× the maximum cloud column calculated by Wordsworth *et al.* (2013). Overall, the impact of clouds on their own on UV-sensitive photochemistry is expected to be modest.

If young Mars were indeed cold and dry, then one might expect it to have been dusty, as it is today. The modern martian dust optical depth ranges from $\tau_d \sim 0.2$ to 2, with higher values achieved during dust storms (Smith *et al.,* 2002; Lemmon *et al.*, 2015). Higher dust loadings may have been possible when the atmosphere was thicker. Figure 14 presents the dose rates as a function of τ_d and pCO_2, for SZA = 0 and A corresponding to desert. Figure 15 presents the dose rates as a function of τ_d and CO_2 cloud optical depth, for SZA = 0 and A corresponding to desert.
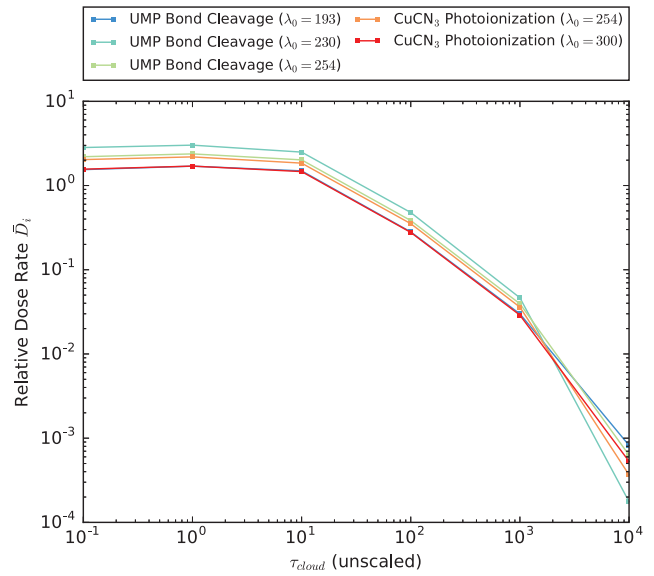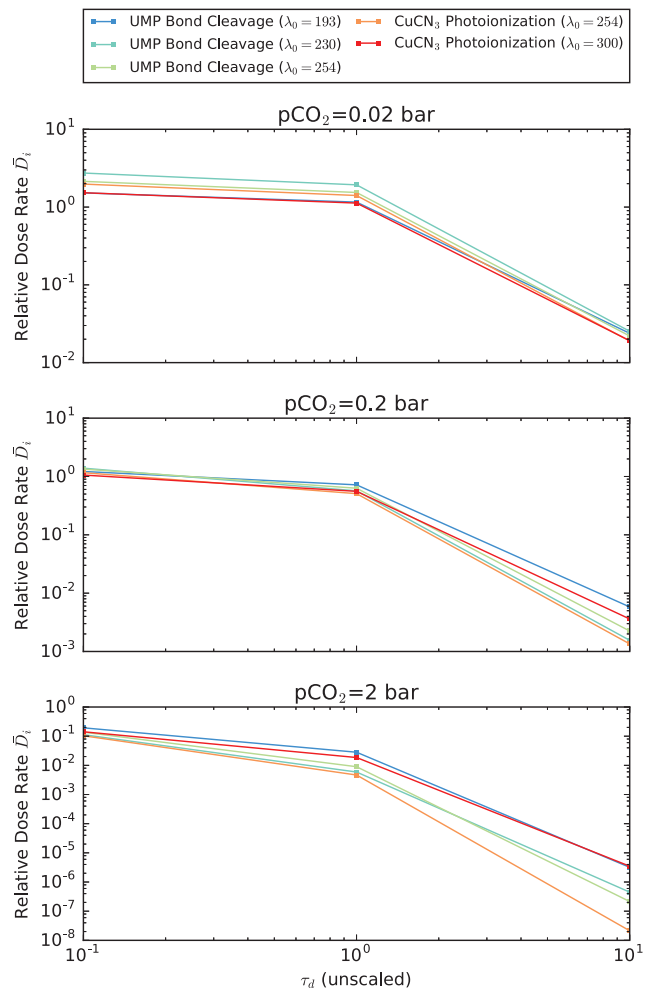

FIG. 14. UV dose rates $\overline{D_i}$ for dusty CO_2-H_2O atmospheres as a function of pCO_2 and τ_d ($T_0 = 250$ K, SZA = 0, A corresponding to desert).

FIG. 15. UV dose rates $\overline{D_i}$ for dusty CO_2-H_2O atmospheres with a CO_2 cloud deck emplaced, as a function of τ_d and τ_{cloud} ($T_0 = 250$ K, $pCO_2 = 0.02$, SZA $= 0$, A corresponding to desert).

Unlike CO_2 and H_2O ice and gas, dust absorbs across the UV waveband. Further, this absorption can be dramatically increased in highly scattering atmospheres due to enhanced effective path length due to multiple scattering effects. Consequently, dust can dramatically suppress UV fluence and hence photochemistry, especially for thick and/or cloudy atmospheres. For $\tau_d \geq 10$, dose rates are suppressed by 2–8 orders of magnitude, depending on atmospheric pressure and cloud thickness. Dust of thickness $\tau_d = 1$ provides minimal suppression for $pCO_2 \leq 0.2$ bar or $\tau_{cloud} < 100$, but for $pCO_2 \geq 2$ bar or $\tau_{cloud} \geq 1000$ it can suppress dose rates by orders of magnitude. Dust of thickness $\tau_d \leq 0.1$ does not significantly alter dose rates across the explored parameter space. Overall, dust can significantly alter dose rates if it is present at high levels (greater than that seen for modern martian dust storms) or if it is present at levels comparable to the modern average but embedded in a thick atmosphere or underlying thick clouds.

We considered the hypothesis that attenuation due to dust might differentially affect the stressor and eustressor pathways. That is, we considered the possibility that the eustressor reaction rates might fall off faster (or slower) than the stressor reaction rates with attenuation due to dust. Since the stressor pathway measures destruction of RNA monomers and the eustressor pathway measures a process important to the synthesis of key RNA precursors, this means that environments that favor the eustressor pathway over the stressor pathway are a more favorable venue for abiogenesis than the reverse, in the RNA world hypothesis. This argument assumes that these particular stressor and eustressor processes were important in the prebiotic world. They might not have been. However, we expect other photochemical stressor and eustressor processes to behave in generally similar ways to these processes. For example, we generally expect the QY of prebiotic molecular destruction to decrease with increasing wavelength because of decreased photon energy compared to bond strength. Similarly, regardless of the solvated electron source (*e.g.,* HS⁻ as opposed to tricyanocuprate), we expect the QY to go approximately as a step function in wavelength. We therefore suggest that results derived from these pathways may generalize to other processes, though a detailed comparison is required to rule on this hypothesis.

To assess the hypothesis that a dusty Mars might be less (or more) clement for abiogenesis than a nondusty Mars as measured by our stressor (UMP-X) and eustressor (CuCN3-Y) pathways, we calculated $\overline{D}_{\text{UMP}-X}/\overline{D}_{\text{CuCN3-Y}}$. We calculated this quantity for $pCO_2 = 2$ bar (no clouds) and $\tau_{\text{cloud}} = 1000$ ($pCO_2 = 0.02$ bar) for $\tau_d = 0.1$–10. If these ratios rise with τ_d, it means that the stressor pathway is relatively favored by dusty atmospheres; if they fall, it means that the stressor pathway is relatively disfavored by dusty atmospheres.

Figure 16 presents these calculations. Dust attenuation on its own is relatively flat at CO_2-scattering wavelengths, as is cloud attenuation. Consequently, dusty/cloudy atmospheres tend to reduce UV fluence in a spectrally flat manner and favor neither the stressor nor the eustressor pathway. On the other hand, in a thick CO_2 atmosphere, the scattering optical depth and, hence, amplification of dust absorption increase as wavelength decreases. Consequently, the dose rate ratio does change with increasing τ_d. However, the direction of the change is sensitive to the value of λ_0, the ionization threshold for the tricyanocuprate ionization process, and the magnitude is further sensitive to the value of λ_0 for the UMP cleavage process. We consequently conclude it is possible that thick, dusty atmospheres might be more or less clement for abiogenesis than nondusty atmospheres, but determining which requires wavelength-dependent measurements of the QYs of these chemical processes in the laboratory.

5.2. Highly reducing atmospheres

Recent work suggests that, if the reduced gases H_2 and/or CH_4 were present at elevated levels in a thick (~ 1 bar) atmosphere, collision-induced absorption (CIA) due to the interaction of these gases with CO_2 might provide enough greenhouse warming to elevate mean Noachian temperatures above freezing (Ramirez *et al.,* 2014; Wordsworth *et al.,* 2017). Ramirez *et al.* (2014) found that global mean surface temperatures exceeded 273 K for $P_0 \geq 3$ bar and $[H_2] \geq 0.05$, with higher concentrations of H_2 required for lower P_0. More recently, Wordsworth *et al.* (2017) used new *ab initio* calculations of H_2-CO_2 and CH_4-CO_2 CIA to show
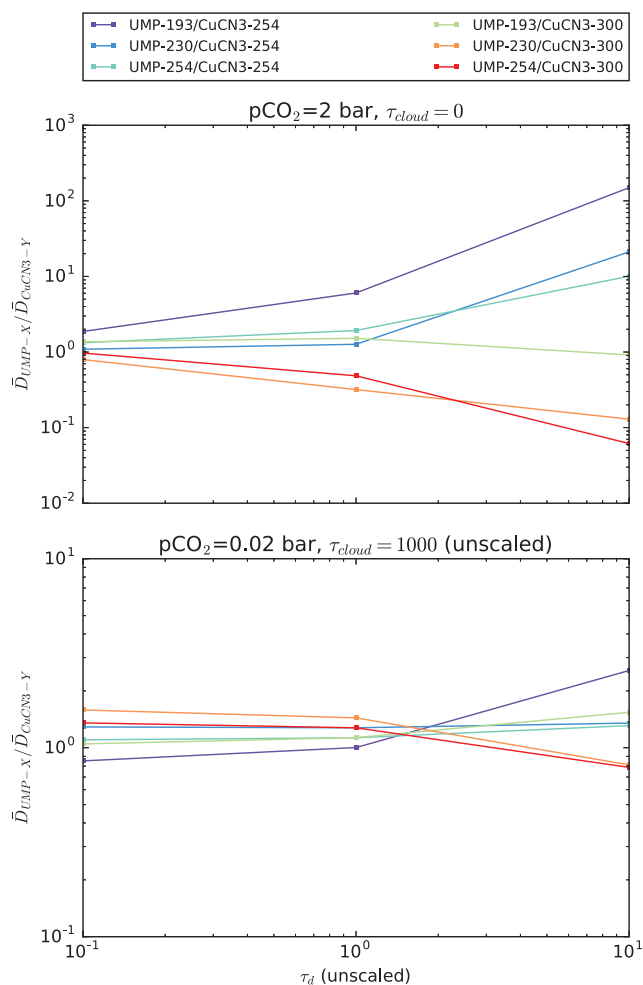
FIG. 16. Ratio of stressor dose rates UMP-X divided by eustressor dose rates UMP-Y for dusty CO_2-H_2O atmospheres, as a function of τ_d ($T_0 = 250$ K, SZA $= 0$, A corresponding to desert). The atmospheres are highly scattering, either because of high pCO_2 or thick CO_2 clouds. Lower ratios imply a more favorable environment for abiogenesis as measured by these two photoprocesses.

that earlier estimates of the CIA were underestimated and that 2–10% levels of CH_4 or H_2 in a >1.25 bar atmosphere could elevate planetary mean temperatures over freezing. While it is unclear whether such high reducing conditions can be sustained in the steady state, this scenario remains an intriguing avenue to a Noachian Mars with conditions at least transiently globally clement for liquid water and prebiotic chemistry (Batalha *et al.*, 2015; Wordsworth *et al.*, 2017).

H_2 is spectrally inert at UV wavelengths compared to CO_2. Based on the constraints on H_2 absorption we found (Victor and Dalgarno, 1969; Backx *et al.*, 1976), the contribution of H_2 to atmospheric absorption and scattering is negligible for H_2 mixing ratios of 0–0.1. Similarly, CH_4 does not absorb at wavelengths longer than 165 nm (Au *et al.*, 1993; Chen and Wu, 2004). Hence, its absorption is highly degenerate with CO_2, and its presence at the levels suggested by Wordsworth *et al.* (2017) does not impact the UV surface environment. Photo-

chemically generated hydrocarbon hazes require CH_4/CO_2 ratios of >0.1 and are consequently expected to be thin or nonexistent in this scenario (DeWitt *et al.*, 2009). Consequently, the UV surface environment in an H_2- or CH_4-rich atmosphere should be similar to the p$CO_2 = 2$ bar case discussed in Section 5.1.

5.3. Highly volcanic Mars (CO_2-H_2O-SO_2/H_2S atmosphere)

We have so far considered atmospheres with CO_2 and H_2O as their dominant photoactive gaseous species. However, other gases have been proposed as significant constituents of the martian atmosphere. In particular, Halevy *et al.* (2007) suggested that the lack of massive carbonate deposits on Mars could have been explained if, during epochs of high volcanism on young Mars, SO_2 built up to the ~ 1–100 ppm level. At such levels, Halevy *et al.* (2007) found that SO_2 would supplant CO_2 as the agent regulating global chemistry and climate, inhibiting massive carbonate precipitation in the process. Halevy and Head (2014) further argued that enhanced radiative forcing from high SO_2 levels
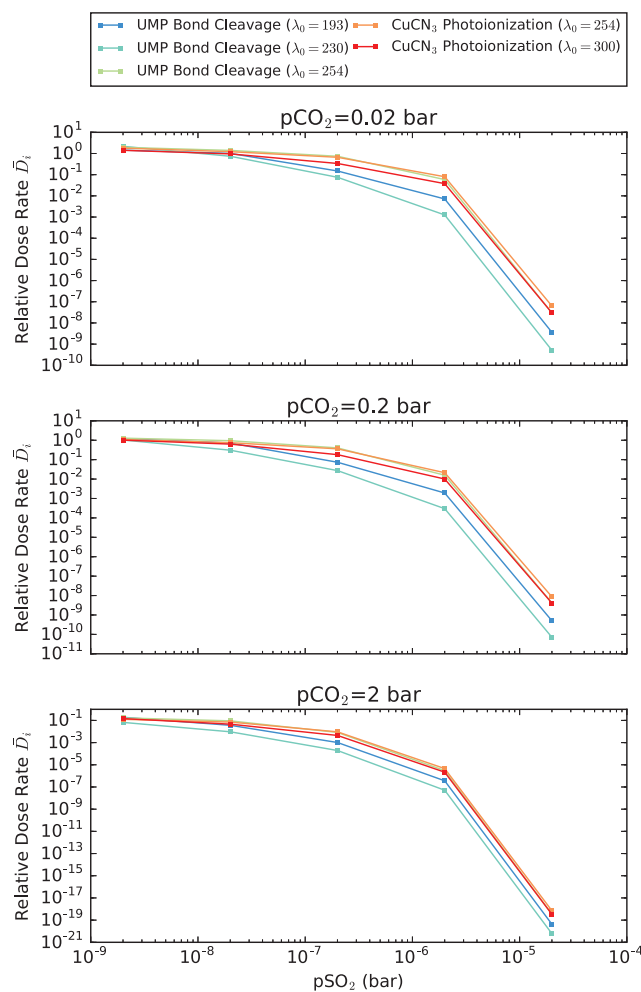

FIG. 17. UV dose rates $\overline{D_i}$ for CO_2-H_2O-SO_2 atmospheres as a function of pCO_2 and pSO_2 ($T_0 = 250$ K, SZA $= 0$, A corresponding to desert).

could transiently raise mean surface temperatures at the subsolar point (assuming no horizontal heat transport) above the freezing point of water, explaining the observed fluvial features. Halevy and Head (2014) calculated that SO_2 mixing ratios $\gtrsim 10$ ppm (1 bar atmosphere) could have been possible during, for example, the emplacement of the martian volcanic plains. While the impact of SO_2 on martian carbonates and climate remains debated (*e.g.,* Niles *et al.,* 2013; Kerber *et al.,* 2015), it is plausible that Noachian Mars may have been characterized by at least transiently high SO_2 levels due to higher volcanic outgassing rates.

We consequently sought to explore the impact of elevated levels of SO_2 on the UV surface environment and hence prebiotic chemistry. Figure 17 presents the dose rates calculated for a clear-sky atmosphere with varying pSO_2 and pCO_2. Figure 18 presents the dose rates calculated for an atmosphere with $pCO_2 = 0.02$ bar (optically thin at scattering wavelengths) but varying levels of CO_2 clouds. In both cases, SZA = 0, and A corresponds to desert.

SO_2 is a far broader, stronger UV absorber than either CO_2 or H_2O; consequently, its presence can exert a dramatic impact on UV surface radiance and photochemistry rates. As
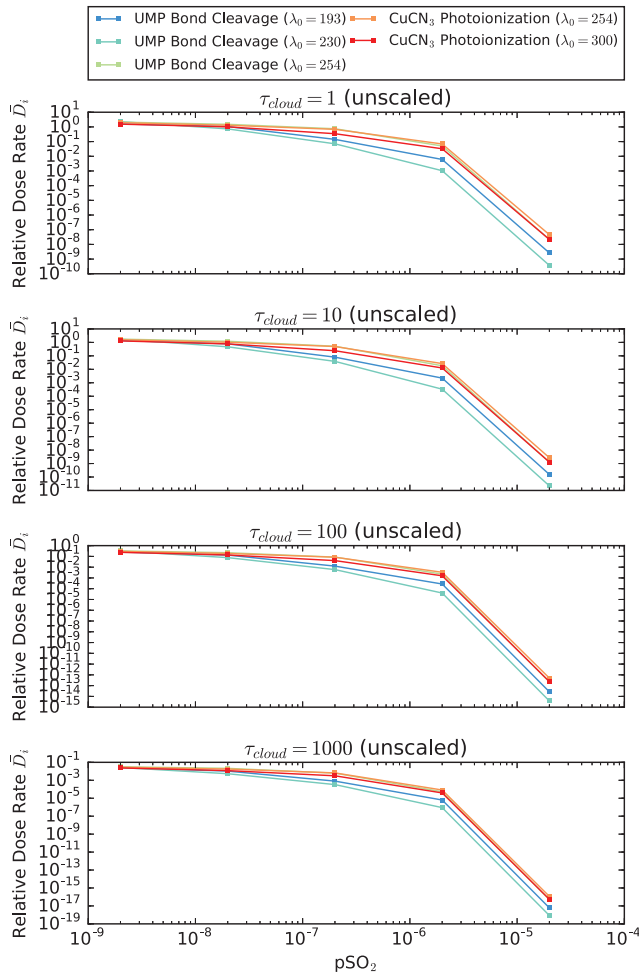
with dust, multiple scattering from other atmospheric constituents can amplify SO_2 absorption. For $pCO_2 \leq 0.2$ bar, $pSO_2 \geq 2 \times 10^{-6}$ bar is required to suppress dose rates to $\overline{D_i} < 0.1$, whereas for $pCO_2 \geq 2$ bar, $pSO_2 \geq 2 \times 10^{-7}$ bar is sufficient. Similarly, for $\tau_{cloud} \leq 10$, $pSO_2 \geq 2 \times 10^{-6}$ bar is required to suppress dose rates to $\overline{D_i} < 0.1$, whereas for $\tau_{cloud} \geq 100$, $pSO_2 \geq 2 \times 10^{-7}$ bar is sufficient. For $pSO_2 \geq 2 \times 10^{-5}$ bar, UV-sensitive prebiotic photochemistry is strongly quenched.

As with dust, we considered the hypothesis that attenuation from SO_2 might have a differential impact on the eustressor and stressor pathways. We calculated $\overline{D}_{UMP-X}/\overline{D}_{CuCN3-Y}$ for $pCO_2 = 2$ bar (no clouds) and $\tau_{cloud} = 1000$ ($pCO_2 = 0.02$ bar) for a broad range of pSO_2. This calculation is presented in Fig. 19. We note that, regardless of assumption on λ_0, as pSO_2 increases from 2×10^{-7} to 2×10^{-5} bar, the eustressor pathway is favored over the stressor pathways by as much as 2 orders of magnitude (dependent on λ_0). We conclude that it seems
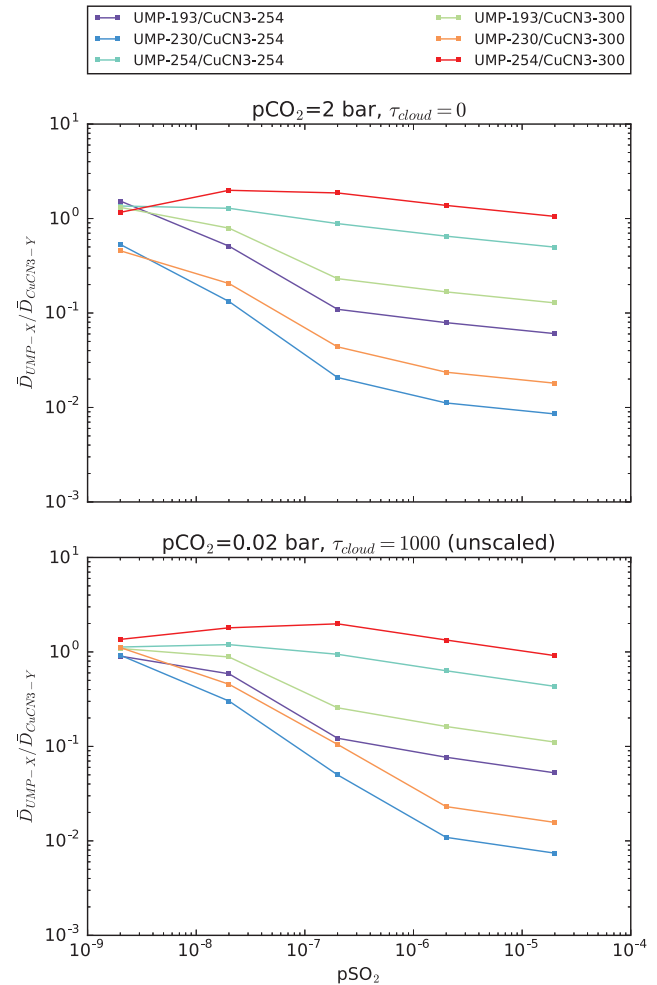

FIG. 18. UV dose rates $\overline{D_i}$ for CO_2-H_2O-SO_2 atmospheres with a CO_2 cloud deck emplaced, as a function of pSO_2 and τ_{cloud} ($T_0 = 250$ K, $pCO_2 = 0.02$, SZA = 0, A corresponding to desert).

FIG. 19. Ratio of stressor dose rates UMP-X divided by eustressor dose rates UMP-Y for CO_2-H_2O-SO_2 atmospheres, as a function of pSO_2 ($T_0 = 250$ K, SZA = 0, A corresponding to desert). The atmospheres are highly scattering, either because of high pCO_2 or thick CO_2 clouds. Lower ratios imply a more favorable environment for abiogenesis as measured by these two photoprocesses.

plausible that high-SO_2 planetary atmospheres have a UV throughput more clement for abiogenesis compared to low-SO_2 atmospheres under the assumption that the stressor and eustressor pathways we have identified were important. However, better measurements of the spectral QY of these photoprocesses are required to confirm and quantify the magnitude of this effect.

While Halevy and Head (2014) focused on the abundance of SO_2 in the martian atmosphere, H_2S is emitted in equal proportion by the more reduced martian mantle in the work of Halevy *et al.* (2007). Hu *et al.* (2013) modeled the atmospheric composition as a function of sulfur emission rate for a 1 bar CO_2 atmosphere assuming equipartition of the outgassed sulfur between SO_2 and H_2S, irradiated by a G2V star at a distance of 1.3 AU. They found H_2S concentrations to be even higher than SO_2 concentrations, by over an order of magnitude at high S emission rates. H_2S is also a stronger, broader UV absorber than CO_2 or H_2O. Consequently, we sought to explore the impact of elevated levels of H_2S on the UV surface environment and prebiotic photochemistry.

Figure 20 presents the dose rates calculated for a clear-sky atmosphere with varying pH_2S and pCO_2. Figure 21
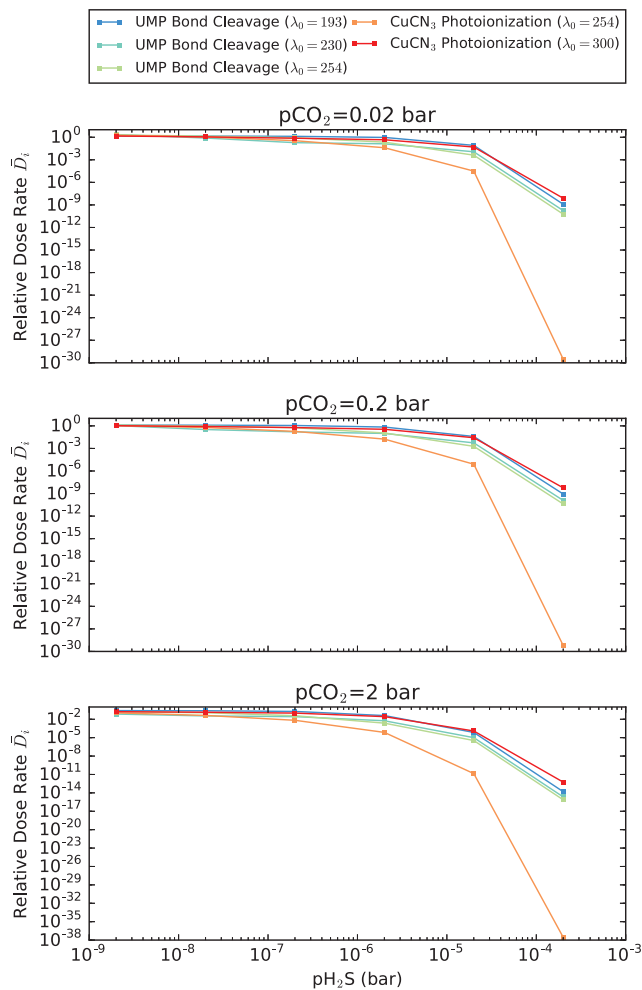

FIG. 20. UV dose rates $\overline{D_i}$ for CO_2-H_2O-H_2S atmospheres as a function of pCO_2 and pH_2S ($T_0 = 250\,K$, SZA = 0, A corresponding to desert).
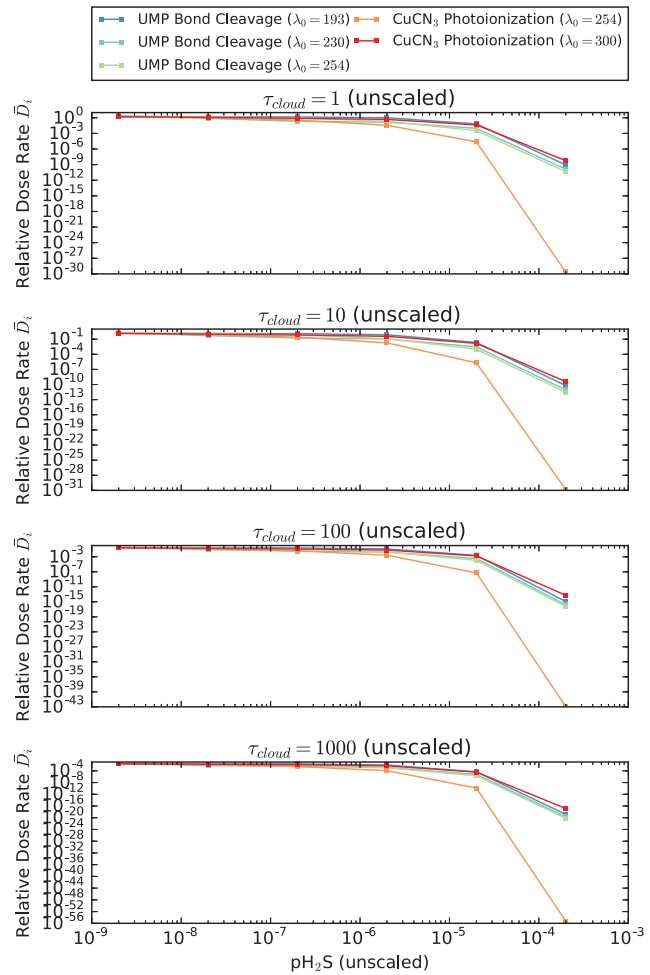
FIG. 21. UV dose rates $\overline{D_i}$ for CO_2-H_2O-H_2S atmospheres with a CO_2 cloud deck emplaced, as a function of pH_2S and τ_{cloud} ($T_0 = 250\,K$, $pCO_2 = 0.02\,bar$, SZA = 0, A corresponding to desert).

presents the dose rates calculated for an atmosphere with $pCO_2 = 0.02\,bar$ (optically thin at scattering wavelengths) but varying levels of CO_2 clouds. In both cases, SZA = 0, and A corresponds to desert. As with SO_2 and dust, highly scattering atmospheres can amplify H_2S absorption. For $pCO_2 \leq 0.2\,bar$, $\overline{D_i} < 0.1$ for $pH_2S \geq 2 \times 10^{-5}\,bar$; but for $pCO_2 \geq 2\,bar$, $\overline{D_i} < 0.1$ for $pH_2S \geq 2 \times 10^{-6}\,bar$. Similarly, for $\tau_{cloud} \leq 10$, $\overline{D_i} < 0.1$ for $pH_2S \geq 2 \times 10^{-5}\,bar$; but for $\tau_{cloud} \geq 100$, $\overline{D_i} \lesssim 0.1$ for $pH_2S \geq 2 \times 10^{-6}\,bar$. For $pH_2S \geq 2 \times 10^{-4}\,bar$, surface photochemistry is strongly quenched regardless of atmospheric state.

We again considered the hypothesis that H_2S attenuation might have a differential impact on the stressor and eustressor dose rates. We calculated $\overline{D}_{UMP-X}/\overline{D}_{CuCN3-Y}$ for $pCO_2 = 2\,bar$ (no clouds) and $\tau_{cloud} = 1000$ ($pCO_2 = 0.02\,bar$) for a broad range of pH_2S. This calculation is presented in Fig. 22. As in the case of dust in a dense CO_2 atmosphere, the ratios diverge from 1, but in opposite directions depending on the value assumed for λ_0 for photoionization of tricyanocuprate. We conclude that attenuation from H_2S may well have a differential impact on the stressor and eustressor dose rates but that assessing which it favors
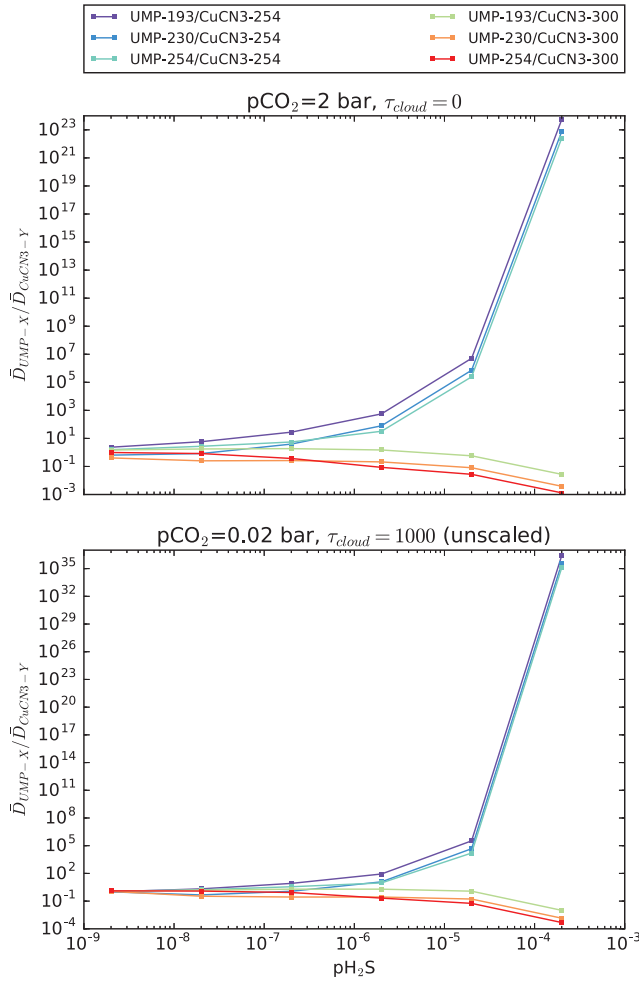
FIG. 22. Ratio of stressor dose rates UMP-X divided by eustressor dose rates UMP-Y for CO_2-H_2O-H_2S atmospheres, as a function of pH_2S ($T_0 = 250$ K, SZA $= 0$, A corresponding to desert). The atmospheres are highly scattering, either because of high pCO_2 or thick CO_2 clouds. Lower ratios imply a more favorable environment for abiogenesis as measured by these two photoprocesses.

requires better constraints on the QYs of the photoprocesses, especially the photoionization of tricyanocuprate.

6. Conclusion

We used a two-stream, multilayer radiative transfer model to estimate the UV environment on the surface of 3.9 Ga Mars as a function of atmospheric composition, and explored the implications for prebiotic chemistry. Prebiotic photoreaction rates are within an order of magnitude of the terrestrial values for normative clear-sky CO_2-H_2O atmospheres, which is in agreement with past work (*e.g.*, Cockell, 2000) and suggests that early martian and terrestrial atmospheres featured comparable UV environments. In agreement with prior work, we find shortwave radiation to be effectively attenuated by CO_2 absorption, with fluence $\lesssim 185$ nm removed for $pCO_2 \geq 2 \times 10^{-5}$ bar and fluence < 204 nm removed for $pCO_2 \geq 0.2$

bar. Fluence drops off more slowly in the > 204 nm regime, where neither CO_2 nor H_2O absorb. This is a consequence of random walk statistics in highly scattering regimes and stands in contrast to prior studies (Rontó *et al.*, 2003; Cnossen *et al.*, 2007) that did not account for multiple scattering. The impact of CO_2 and H_2O clouds on their own is similarly muted because they too are pure scatterers in the > 204 nm regime; $\tau_{cloud} \geq 100$ is required to significantly affect surficial reaction rates, comparable to but in excess of the highest patchy cloud optical depths predicted by some 3-D GCM studies (*e.g.*, Wordsworth *et al.*, 2013).

While dense atmospheres and cloud decks only modestly reduce surface fluence on their own, in concert with other absorbers (dust, SO_2, H_2S) they can have a dramatic effect on surface fluence and reaction rates through amplification of the effects of these absorbers. Dust levels of $\tau_d = 1$, only a factor of a few higher than that sustained in the modern atmosphere, could suppress prebiotic reaction rates by orders of magnitude for $pCO_2 \geq 2$ bar or $\tau_{cloud} \geq 1000$, and dust levels of $\tau_d = 10$ would sharply reduce reaction rates independent of the atmospheric state. Similarly, $pSO_2 \geq 10^{-7}$ bar or $pH_2S \geq 2 \times 10^{-6}$ bar is required to significantly reduce reaction rates for $pCO_2 \geq 2$ bar or $\tau_{cloud} \geq 100$, but for less scattering atmospheres, $pSO_2 \geq 10^{-6}$ bar or $pH_2S \geq 2 \times 10^{-5}$ bar is required. $pSO_2 \geq 10^{-5}$ bar or $pH_2S \geq 2 \times 10^{-4}$ bar quenches UV-sensitive photochemistry by many orders of magnitude regardless of other atmospheric conditions.

The absorbers described above have spectrally variable absorption, and prebiotic photochemistry is wavelength-dependent, leading us to speculate whether high abundances of these absorbers, despite suppressing UV-sensitive chemistry generally, might not favor or disfavor eustressor photoprocesses conducive to the origin of life compared to stressor processes that impede life's formation. We compare the relative impact of absorption from dust, SO_2, and H_2S attenuation on two such stressor (cleavage of the N-glycosidic bond of UMP) and eustressor (production of aquated electrons from $CuCN_3^{2-}$) photoprocesses. We find that it is possible for high levels of these absorbers to disproportionately favor one or the other of these photoprocesses. In particular, high SO_2 levels may create an especially favorable environment for abiogenesis, under the assumption that these photoprocesses were important to abiogenesis (so long as enough fluence reaches the ground to power these reactions). However, the magnitude and direction of this effect are sensitive to assumptions about the QY of these processes. Better characterization of the spectral QYs of these processes are required to rule definitively on this question.

A. Appendix

This appendix presents sample atmospheric profiles calculated using the methods in Section 3.2, to illustrate the application of these methods. Figure A1 shows the T/P profiles associated with a sample atmosphere with varying (pCO_2, T_0), where pCO_2 is the surface partial pressure of CO_2. Figure A2 shows the pressure, temperature, and H_2O molar concentration altitude provides
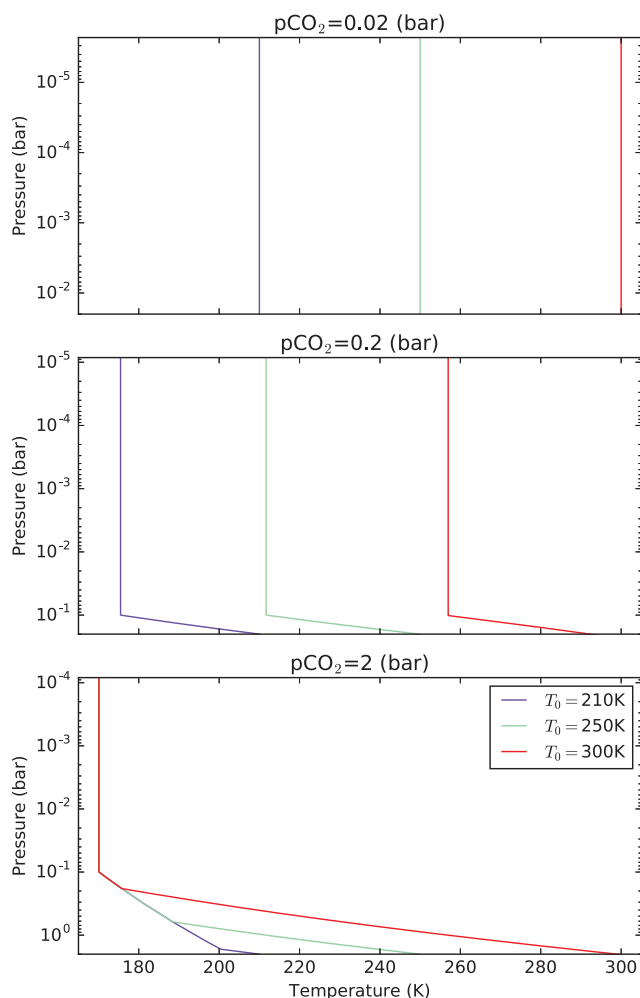
FIG. A1. Sample T/P profiles for CO_2-dominated CO_2-H_2O atmospheres using the methodology in Section 3.2 for $T_0 = 210$, 250, 300 K and $pCO_2 = 0.02$, 0.2, 2 bar. The pressure is the total atmospheric pressure (CO_2 and H_2O).

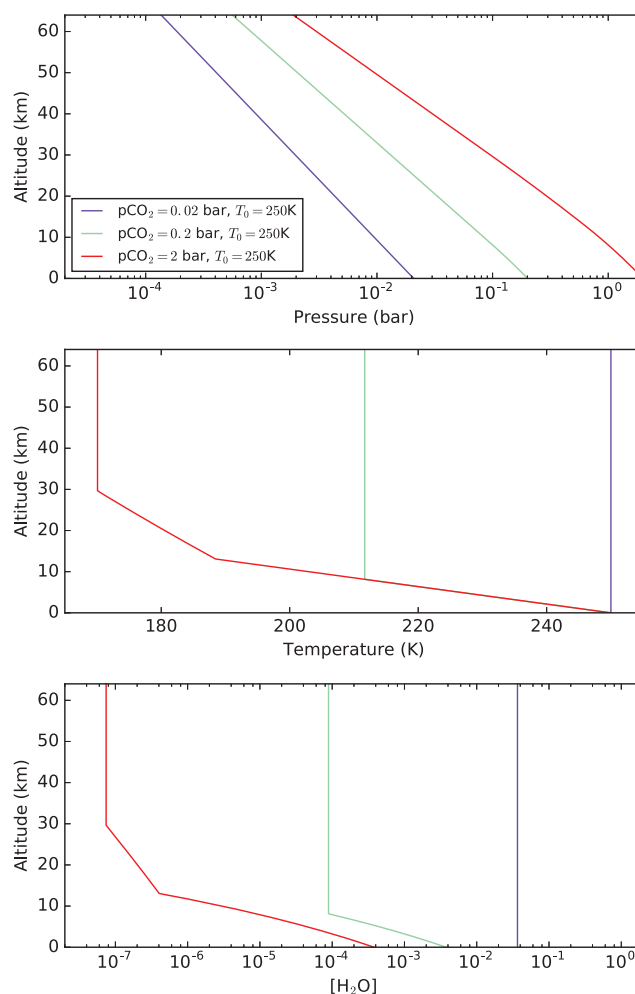**FIG. A2.** Temperature, pressure, and molar concentration of H_2O for atmospheres with $pCO_2 = 0.02$, 0.2, 2 bar and $T_0 = 250$ K.

associated with an atmosphere with $T_0 = 250$ K and varying pCO_2.

Author Disclosure Statement

The authors declare no competing financial interests.

References

Adcock, C.T., Hausrath, E.M., and Forster, P.M. (2013) Readily available phosphate from minerals in early aqueous environments on Mars. *Nat Geosci* 6:824–827.

Au, J.W., Cooper, G., Burton, G.R., Olney, T.N., and Brion, C. (1993) The valence shell photoabsorption of the linear alkanes, C_nH_{2n+2} ($n = 1$–8): absolute oscillator strengths (7–220 eV). *Chem Phys* 173:209–239.

Backx, C., Wight, G.R., and Van der Wiel, M.J. (1976) Oscillator strengths (10–70 eV) for absorption, ionization and dissociation in H_2, HD and D_2, obtained by an electron-ion coincidence method. *J Phys B At Mol Opt Phys* 9:315–331.

Batalha, N., Domagal-Goldman, S.D., Ramirez, R., and Kasting, J.F. (2015) Testing the early Mars H_2-CO_2 greenhouse hypothesis with a 1-D photochemical model. *Icarus* 258:337–349.

Benner, S.A. (2013) Planets, minerals and life's origin. *Mineral Mag* 77:686.

Benner, S.A. and Kim, H.-J. (2015) The case for a martian origin for Earth life. *Proc SPIE* 9606, doi:10.1117/12.2192890.

Benner, S.A., Kim, H.-J., Kim, M.-J., and Ricardo, A. (2010) Planetary organic chemistry and the origins of biomolecules.

Cold Spring Harb Perspect Biol 2, doi:10.1101/cshperspect.a003467.

Bohren, C.F. (1987) Multiple scattering of light and some of its observable consequences. *Am J Phys* 55:524–533.

Bristow, T.F., Bish, D.L., Vaniman, D.T., Morris, R.V., Blake, D.F., Grotzinger, J.P., Rampe, E.B., Crisp, J.A., Achilles, C.N., Ming, D.W., Ehlmann, B.L., King, P.L., Bridges, J.C., Eigenbrode, J.L., Sumner, D.Y., Chipera, S.J., Moorokian, J.M., Treiman, A.H., Morrison, S.M., Downs, R.T., Farmer, J.D., Des Marais, D., Sarrazin, P., Floyd, M.M., Mischna, M.A., and McAdam, A.C. (2015) The origin and implications of clay minerals from Yellowknife Bay, Gale Crater, Mars. *Am Mineral* 100:824–836.

Chen, F. and Wu, C. (2004) Temperature-dependent photoabsorption cross sections in the VUV-UV region. I. Methane and ethane. *J Quant Spectrosc Radiat Transf* 85: 195–209.

Claire, M.W., Sheets, J., Cohen, M., Ribas, I., Meadows, V.S., and Catling, D.C. (2012) The evolution of solar flux from 0.1 nm to 160 μm: quantitative estimates for planetary studies. *Astrophys J* 757, doi:10.1088/0004-637X/757/1/95.

Cnossen, I., Sanz-Forcada, J., Favata, F., Witasse, O., Zegers, T., and Arnold, N.F. (2007) Habitat of early life: solar X-ray and UV radiation at Earth's surface 4–3.5 billion years ago. *J Geophys Res: Planets* 112, doi:10.1029/2006JE002784.

Cockell, C. (2000) The ultraviolet history of the terrestrial planets: implications for biological evolution. *Planet Space Sci* 48:203–214.

Cockell, C.S. (1999) Carbon biochemistry and the ultraviolet radiation environments of F, G, and K main sequence stars. *Icarus* 141:399–407.

Cockell, C.S. (2002) Photobiological uncertainties in the Archaean and post-Archaean world. *International Journal of Astrobiology* 1:31–38.

Colaprete, A. and Toon, O.B. (2003) Carbon dioxide clouds in an early dense martian atmosphere. *J Geophys Res: Planets* 108, doi:10.1029/2002JE001967.

DeWitt, H.L., Trainer, M.G., Pavlov, A.A., Hasenkopf, C.A., Aiken, A.C., Jimenez, J.L., McKay, C.P., Toon, O.B., and Tolbert, M.A. (2009) Reduction in haze formation rate on prebiotic Earth in the presence of hydrogen. *Astrobiology* 9:447–453.

Fanale, F.P., Salvail, J.R., Banerdt, W.B., and Saunders, R.S. (1982) Mars—the regolith-atmosphere-cap system and climate change. *Icarus* 50:381–407.

Forget, F. and Pierrehumbert, R.T. (1997) Warming early Mars with carbon dioxide clouds that scatter infrared radiation. *Science* 278:1273–1276.

Forget, F., Hourdin, F., Fournier, R., Hourdin, C., Talagrand, O., Collins, M., Lewis, S.R., Read, P.L., and Huot, J.-P. (1999) Improved general circulation models of the martian atmosphere from the surface to above 80 km. *J Geophys Res: Planets* 104:24155–24175.

Forget, F., Wordsworth, R., Millour, E., Madeleine, J.-B., Kerber, L., Leconte, J., Marcq, E., and Haberle, R.M. (2013) 3D modelling of the early martian climate under a denser CO_2 atmosphere: temperatures and CO_2 ice clouds. *Icarus* 222:81–99.

Fox, G.K., Code, A.D., Anderson, C.M., Babler, B.L., Bjorkman, K.S., Johnson, J.J., Meade, M.R., Nordsieck, K.H., Sanders, W.T., Weitenbeck, A.J., and Zellner, N.E.B. (1997) Solar System observations by the Wisconsin Ultraviolet Photopolarimeter experiment. I. The first ultraviolet linear spectropolarimetry of Mars. *Astron J* 113:1152–1157.

Gollihar, J., Levy, M., and Ellington, A.D. (2014) Many paths to the origin of life. *Science* 343:259–260.

Grotzinger, J.P., Gupta, S., Malin, M.C., Rubin, D.M., Schieber, J., Siebach, K., Sumner, D.Y., Stack, K.M., Vasavada, A.R., Arvidson, R.E., Calef, F., Edgar, L., Fischer, W.F., Grant, J.A., Griffes, J., Kah, L.C., Lamb, M.P., Lewis, K.W., Mangold, N., Minitti, M.E., Palucis, M., Rice, M., Williams, R.M.E., Yingst, R.A., Blake, D., Blaney, D., Conrad, P., Crisp, J., Dietrich, W.E., Dromart, G., Edgett, K.S., Ewing, R.C., Gellert, R., Hurowitz, J.A., Kocurek, G., Mahaffy, P., McBride, M.J., McLennan, S.M., Mischna, M., Ming, D., Milliken, R., Newsom, H., Oehler, D., Parker, T.J., Vaniman, D., Wiens, R.C., and Wilson, S.A. (2015) Deposition, exhumation, and paleoclimate of an ancient lake deposit, Gale Crater, Mars. *Science* 350, doi:10.1126/science.aac7575.

Gurzadyan, G.G. and Görner, H. (1994) Damage to uracil- and adenine-containing bases, nucleosides, nucleotides and polynucleotides: quantum yields on irradiation at 193 and 254 nm. *Photochem Photobiol* 60:323–332.

Halevy, I. and Head, J.W., III. (2014) Episodic warming of early Mars by punctuated volcanism. *Nat Geosci* 7:865–868.

Halevy, I., Zuber, M.T., and Schrag, D.P. (2007) A sulfur dioxide climate feedback on early Mars. *Science* 318:1903–1907.

Hansen, G.B. (1997) The infrared absorption spectrum of carbon dioxide ice from 1.8 to 333 μm. *J Geophys Res* 102: 21569–21588.

Hansen, G.B. (2005) Ultraviolet to near-infrared absorption spectrum of carbon dioxide ice from 0.174 to 1.8 μm. *J Geophys Res: Planets* 110, doi:10.1029/2005JE002531.

Hansen, J.E. and Travis, L.D. (1974) Light scattering in planetary atmospheres. *Space Sci Rev* 16:527–610.

Herd, C.D.K., Borg, L.E., Jones, J.H., and Papike, J.J. (2002) Oxygen fugacity and geochemical variations in the martian basalts: implications for martian basalt petrogenesis and the oxidation state of the upper mantle of Mars. *Geochim Cosmochim Acta* 66:2025–2036.

Hoekzema, N.M., Garcia-Comas, M., Stenzel, O.J., Grieger, B., Markiewicz, W.J., Gwinner, K., and Keller, H.U. (2010) Optical depth and its scale-height in Valles Marineris from HRSC stereo images. *Earth Planet Sci Lett* 294:534–540.

Horváth, A., Papp, S., and Décsy, Z. (1984) Formation of aquated electrons and the individual quantum yields for photoactive species in the Cu (I)KCNH$_2$O system. *Journal of Photochemistry* 24:331–339.

Hu, R., Seager, S., and Bains, W. (2012) Photochemistry in terrestrial exoplanet atmospheres. I. Photochemistry model and benchmark cases. *Astrophys J* 761, doi:10.1088/0004-637X/761/2/166.

Hu, R., Seager, S., and Bains, W. (2013) Photochemistry in terrestrial exoplanet atmospheres. II. H$_2$S and SO$_2$ photochemistry in anoxic atmospheres. *Astrophys J* 769, doi:10.1088/0004-637X/769/1/6.

Joseph, J.H., Wiscombe, W.J., and Weinman, J.A. (1976) The delta-Eddington approximation for radiative flux transfer. *Journal of Atmospheric Sciences* 33:2452–2459.

Kasting, J.F. (1991) CO_2 condensation and the climate of early Mars. *Icarus* 94:1–13.

Kerber, L., Forget, F., and Wordsworth, R. (2015) Sulfur in the early martian atmosphere revisited: experiments with a 3-D global climate model. *Icarus* 261:133–148.

Kirschvink, J.L. and Weiss, B.P. (2002) Mars, panspermia, and the origin of life: where did it all begin. *Palaeontologia Electronica* 4:8–15.

Kylling, A., Stamnes, K., and Tsay, S.-C. (1995) A reliable and efficient two-stream algorithm for spherical radiative transfer: documentation of accuracy in realistic layered media. *J Atmosph Chem* 21:115–150.

Lemmon, M.T., Wolff, M.J., Bell, J.F., III, Smith, M.D., Cantor, B.A., and Smith, P.H. (2015) Dust aerosol, clouds, and the atmospheric optical depth record over 5 Mars years of the Mars Exploration Rover mission. *Icarus* 251:96–111.

Madronich, S. (1987) Photodissociation in the atmosphere: 1. Actinic flux and the effects of ground reflections and clouds. *J Geophys Res: Atmospheres* 92:9740–9752.

Magnani, C.J. (2015) Life's first steps: exploring the feasibility of prebiotic chemical reactions through ultraviolet dependence. AB thesis, Harvard University, Cambridge, MA.

Maher, K.A. and Stevenson, D.J. (1988) Impact frustration of the origin of life. *Nature* 331:612–614.

Mayer, B., Kylling, A., Madronich, S., and Seckmeyer, G. (1998) Enhanced absorption of UV radiation due to multiple scattering in clouds: experimental evidence and theoretical explanation. *J Geophys Res* 103, doi:10.1029/98JD02676.

Miller, T.M. (2009) Atomic and molecular polarizabilities. In *CRC Handbook of Chemistry and Physics,* 90th ed., edited by D.R. Lide, CRC Press, Boca Raton, FL.

Mishra, M.K., Chauhan, P., Singh, R., Moorthi, S.M., and Sarkar, S.S. (2016) Estimation of dust variability and scale height of atmospheric optical depth (AOD) in the Valles Marineris on Mars by Indian Mars Orbiter Mission (MOM) data. *Icarus* 265:84–94.

Mulkidjanian, A.Y., Cherepanov, D.A., and Galperin, M.Y. (2003) Survival of the fittest before the beginning of life: selection of the first oligonucleotide-like polymers by UV light. *BMC Evol Biol* 3, doi:10.1186/1471-2148-3-12.

Niles, P.B., Catling, D.C., Berger, G., Chassefière, E., Ehlmann, B.L., Michalski, J.R., Morris, R., Ruff, S.W., and Sutter, B. (2013) Geochemistry of carbonates on Mars: implications for climate history and nature of aqueous environments. *Space Sci Rev* 174:301–328.

Pang, K. and Ajello, J.M. (1977) Complex refractive index of martian dust—wavelength dependence and composition. *Icarus* 30:63–74.

Parkinson, W.H., Rufus, J., and Yoshino, K. (2003) Absolute absorption cross section measurements of CO_2 in the wavelength region 163–200 nm and the temperature dependence. *Chem Phys* 290:251–256.

Patel, B.H., Percivalle, C., Ritson, D.J., Duffy, C.D., and Sutherland, J.D. (2015) Common origins of RNA, protein and lipid precursors in a cyanosulfidic protometabolism. *Nat Chem* 7:301–307.

Pierrehumbert, R.T. (2010) *Principles of Planetary Climate,* Cambridge University Press, Cambridge, UK.

Powner, M.W., Gerland, B., and Sutherland, J.D. (2009) Synthesis of activated pyrimidine ribonucleotides in prebiotically plausible conditions. *Nature* 459:239–242.

Ramirez, R.M., Kopparapu, R., Zugger, M.E., Robinson, T.D., Freedman, R., and Kasting, J.F. (2014) Warming early Mars with CO_2 and H_2. *Nat Geosci* 7:59–63.

Ranjan, S. and Sasselov, D.D. (2016) Influence of the UV environment on the synthesis of prebiotic molecules. *Astrobiology* 16:68–88.

Ranjan, S. and Sasselov, D.D. (2017) Constraints on the early terrestrial surface UV environment relevant to prebiotic chemistry. *Astrobiology* 17:169–204.

Rapf, R.J. and Vaida, V. (2016) Sunlight as an energetic driver in the synthesis of molecules necessary for life. *Phys Chem Chem Phys* 18:20067–20084.

Ritson, D. and Sutherland, J.D. (2012) Prebiotic synthesis of simple sugars by photoredox systems chemistry. *Nat Chem* 4:895–899.

Robinson, T.D. and Catling, D.C. (2014) Common 0.1 bar tropopause in thick atmospheres set by pressure-dependent infrared transparency. *Nat Geosci* 7:12–15.

Rontó, G., Bérces, A., Lammer, H., Cockell, C.S., Molina-Cuberos, G.J., Patel, M.R., and Selsis, F. (2003) Solar UV irradiation conditions on the surface of Mars. *Photochem Photobiol* 77:34–40.

Rosenberg, R., Abu Haija, M., and Ryan, P. (2008) Chiral-selective chemistry induced by spin-polarized secondary electrons from a magnetic substrate. *Phys Rev Lett* 101, doi:10.1103/PhysRevLett.101.178301.

Rugheimer, S., Segura, A., Kaltenegger, L., and Sasselov, D. (2015) UV surface environment of Earth-like planets orbiting FGKM stars through geological evolution. *Astrophys J* 806, doi:10.1088/0004-637X/806/1/137.

Sagan, C. (1973) Ultraviolet selection pressure on the earliest organisms. *J Theor Biol* 39:195–200.

Sarker, P.K., Takahashi, J.-i., Obayashi, Y., Kaneko, T., and Kobayashi, K. (2013) Photo-alteration of hydantoins against UV light and its relevance to prebiotic chemistry. *Adv Space Res* 51:2235–2240.

Segura, A., Meadows, V.S., Kasting, J.F., Crisp, D., and Cohen, M. (2007) Abiotic formation of O_2 and O_3 in high-CO_2 terrestrial atmospheres. *Astron Astrophys* 472:665–679.

Sinsheimer, R.L. and Hastings, R. (1949) A reversible photochemical alteration of uracil and uridine. *Science* 110:525–526.

Sleep, N.H., Zahnle, K.J., Kasting, J.F., and Morowitz, H.J. (1989) Annihilation of ecosystems by large asteroid impacts on the early Earth. *Nature* 342:139–142.

Smith, M.D., Conrath, B.J., Pearl, J.C., and Christensen, P.R. (2002) NOTE: Thermal Emission Spectrometer observations of martian planet-encircling dust storm 2001A. *Icarus* 157:259–263.

Stark, G., Yoshino, K., Smith, P.L., and Ito, K. (2007) Photo-absorption cross section measurements of CO_2 between 106.1 and 118.7 nm at 295 and 195 K. *J Quant Spectrosc Radiat Transf* 103:67–73.

Stephenson, J.D., Hallis, L.J., Nagashima, K., and Freeland, S.J. (2013) Boron enrichment in martian clay. *PLoS One* 8, doi:10.1371/journal.pone.0064624.

Tian, F., Kasting, J.F., and Solomon, S.C. (2009) Thermal escape of carbon from the early martian atmosphere. *Geophys Res Lett* 36:L02205.

Toon, O.B., McKay, C.P., Ackerman, T.P., and Santhanam, K. (1989) Rapid calculation of radiative heating rates and photodissociation rates in inhomogeneous multiple scattering atmospheres. *J Geophys Res* 94:16287–16301.

Victor, G.A. and Dalgarno, A. (1969) Dipole properties of molecular hydrogen. *J Chem Phys* 50:2535–2539.

Vincendon, M., Pilorget, C., Gondet, B., Murchie, S., and Bibring, J.-P. (2011) New near-IR observations of mesospheric CO_2 and H_2O clouds on Mars. *J Geophys Res: Planets* 116, doi:10.1029/2011JE003827.

Voet, D., Gratzer, W.B., Cox, R.A., and Doty, P. (1963) Absorption spectra of nucleotides, polynucleotides, and nucleic acids in the far ultraviolet. *Biopolymers* 1:193–208.

Wagner, W. and Pruß, A. (2002) The IAPWS formulation 1995 for the thermodynamic properties of ordinary water substance

for general and scientific use. *J Phys Chem Ref Data* 31:387–535.

Wagner, W., Saul, A., and Pruss, A. (1994) International equations for the pressure along the melting and along the sublimation curve of ordinary water substance. *J Phys Chem Ref Data* 23:515–527.

Warren, S.G. and Brandt, R.E. (2008) Optical constants of ice from the ultraviolet to the microwave: a revised compilation. *J Geophys Res: Atmospheres* 113, doi:10.1029/2007JD009744.

Wolff, M.J., Smith, M.D., Clancy, R.T., Arvidson, R., Kahre, M., Seelos, F., Murchie, S., and Savijärvi, H. (2009) Wavelength dependence of dust aerosol single scattering albedo as observed by the Compact Reconnaissance Imaging Spectrometer. *J Geophys Res: Planets* 114, doi:10.1029/2009JE003350.

Wordsworth, R., Forget, F., Millour, E., Head, J.W., Madeleine, J.-B., and Charnay, B. (2013) Global modelling of the early martian climate under a denser CO_2 atmosphere: water cycle and ice evolution. *Icarus* 222:1–19.

Wordsworth, R., Kalugina, Y., Lokshtanov, S., Vigasin, A., Ehlmann, B., Head, J., Sanders, C., and Wang, H. (2017) Transient reducing greenhouse warming on early Mars. *Geophys Res Lett* 44:665–671.

Wordsworth, R.D. (2016) The climate of early Mars. *Annu Rev Earth Planet Sci* 44:381–408.

Wordsworth, R.D., Kerber, L., Pierrehumbert, R.T., Forget, F., and Head, J.W. (2015) Comparison of ''warm and wet'' and ''cold and icy'' scenarios for early Mars in a 3-D climate model. *J Geophys Res: Planets* 120:1201–1219.

Yoshino, K., Esmond, J.R., Sun, Y., Parkinson, W.H., Ito, K., and Matsui, T. (1996) Absorption cross section measurements of carbon dioxide in the wavelength region 118.7–175.5 nm and the temperature dependence. *J Quant Spectrosc Radiat Transf* 55:53–60.

Zurek, R.W. (1978) Solar heating of the martian dusty atmosphere. *Icarus* 35:196–208.

Address correspondence to:
Sukrit Ranjan
60 Garden Street
Mail Stop 10
Cambridge, MA 02138

E-mail: sranjan@cfa.harvard.edu

Abbreviations Used

CIA = collision-induced absorption
GCM = General Circulation Model
QY = quantum yield
SZA = solar zenith angle
TOA = top-of-atmosphere
UMP = uridine monophosphate